Holocene climate variability of the western Mediterranean: surface water dynamics inferred from calcareous plankton assemblages

Pietro Bazzicalupo[1], Patrizia Maiorano[1], Angela Girone[1], Maria Marino[1], Nathalie Combourieu-Nebout[2], Nicola Pelosi[3], Emília Salgueiro[4,5], Alessandro Incarbona[6]

1 Dipartimento di Scienze della Terra e Geoambientali, Università degli Studi di Bari Aldo Moro, via E. Orabona 4, 70125, Bari, Italy
2 French National Centre for Scientific Research UMR 7194 - Histoire Naturelle de l'Homme Préhistorique, Paris, France
3 Istituto di Scienze Marine (ISMAR) - Consiglio Nazionale delle Ricerche, Calata Porta di Massa, 80133-Napoli, Italy
4 Div. Geologia e Georecursos Marinhos, Instituto Português do Mar e da Atmosfera (IPMA), Lisbon, 1749-077, Portugal
5 Centre of Marine Sciences, Universidade do Algarve, Faro, 8005-139, Portugal.
6 Università di Palermo, Dipartimento di Scienze della Terra e del Mare, Via Archirafi 22, 90134 Palermo, Italy

Keywords
Coccolithophores, Foraminifera, Alboran Sea, Holocene, Paleoclimate, Paleoproductivity, Millennial-centennial scale climate variability

Abstract
A high resolution study (centennial-scale) has been performed on the calcareous plankton assemblage of the Holocene portion of the Ocean Drilling Program Site 976 (Alboran Sea) with the aim to identify main changes in surface water dynamic. The dataset also provided a Seasonal foraminiferal Sea Surface Water Temperatures (SSTs), estimated using the modern analog technique SIMMAX 28, and it was compared with available geochemical and pollen data at the site.
Three main climate shifts were identified: I) The increase in abundance of *Syracosphaera* spp. and *Turborotalita quinqueloba* marks the early Holocene humid phase, during maximum summer insolation and enhanced river runoff. It is concomitant with the expansion of *Quercus,* supporting high humidity on land. It ends at 8.2 ka, registering a sudden temperature and humidity reduction; II) The rise in the abundances of *Florisphaera profunda* and *Globorotalia inflata*, at ca. 8 ka, indicates the development of the modern geostrophic front, gyre circulation and of a deep nutricline following the sea-level rise; III) The increase of small *Gephyrocapsa* and *Globigerina bulloides* at 5.3 ka,

suggests enhanced nutrient availability in surface waters, related to more persistent wind-induced upwelling conditions. Relatively higher winter SST in the last 3.5 kyr favored the increase of *Trilobatus sacculifer,* likely connected to more stable surface water conditions. Over the main trends, a short term cyclicity is registered in coccolithophore productivity during the last 8 kyr. Short periods of increased productivity are in phase with Atlantic waters inflow, and more arid intervals on land. This cyclicity has been related with periods of positive North Atlantic Oscillation (NAO) circulations. Spectral analysis on coccolithophore productivity confirms the occurrence of millennial-scale cyclicity suggesting an external (i.e. solar) and an internal (i.e. atmospheric/oceanic) forcing.

Introduction

An increasing number of climate records reveals that the Holocene has experienced a pervasive millennial- and centennial-scale climate variability (e.g. Jalut et al., 2009; Magny et al., 2013; Mayewski et al., 2004; Walker et al., 2012; Wanner et al., 2015), well-documented in both the North Atlantic (e.g. Bond et al., 2001; Repschläger et al., 2017; Thornalley et al., 2009) and western Mediterranean (e.g. Ausín et al., 2015a; Cacho et al., 2001; Català et al., 2018; Frigola et al., 2007; Jalali et al., 2017, 2016; Nieto-Moreno et al., 2015; Rodrigo-Gámiz et al., 2011). The western Mediterranean Sea is in fact extremely sensitive to the changes experienced in the North Atlantic and is an ideal location for high-frequency climatic investigations, because water mass properties changes and oceanographic and atmospheric circulation oscillations are usually amplified (Cacho et al., 1999, 2001; Català et al., 2018; Frigola et al., 2007, 2008; Jalali et al., 2016; Moreno et al., 2002; Nieto-Moreno et al., 2015; Sierro et al., 2005; Toucanne et al., 2012). The millennial-scale climate variability in the western Mediterranean is reflected in different water column configurations and oceanographic features (e.g. fronts and eddies) that left a clear signature in the calcareous plankton assemblages (Ausín et al., 2015a; Pérez-Folgado et al., 2003, 2004; Sbaffi et al., 2001). During the Holocene, the Alboran Sea experienced relevant oceanographic perturbations, the most important of which was the instauration of the modern geostrophic front and establishment of gyre anticyclonic circulation dynamics, following sea level rising after the last deglaciation (Ausín et al., 2015b; Català et al., 2018; Colmenero-Hidalgo et al., 2004; Heburn and La Violette, 1990; Rohling et al., 1995; Weaver and Pujol, 1988). This important change also marked the end of the Organic Rich Layer 1 (ORL1) deposition in the western Mediterranean (Bárcena et al., 2001; Cacho et al., 2002; Jimenez-Espejo et al., 2007, 2008; Rogerson et al., 2008). Targeting the high frequency oscillations experienced during the Holocene, a growing attention has been focused on the impact of the North Atlantic Oscillation (NAO) atmospheric pattern in the western Mediterranean Sea, in terms of westerlies strength and deep water production, precipitation and river runoff, and coccolithophore

productivity (Ausín et al., 2015a; Fletcher et al., 2012; Frigola et al., 2007; Jalali et al., 2016; Moreno et al., 2005; Smith et al., 2016; Trigo et al., 2004; Zielhofer et al., 2017). However, only a few studies so far have documented the relationship between coccolithophore productivity and atmospheric variability, like the present NAO index (e.g. Ausín et al., 2015a).

In this framework we carried out, over the last 12 ka, at the Ocean Drilling Program (ODP) Site 976, an integrated study between coccolithophores and planktonic foraminifera by a centennial-scale resolution, not available so far in the Alboran Sea. The aim was to reconstruct paleoenvironmental fluctuations in the Alboran Sea and to discuss the mechanisms controlling fossil assemblage and productivity variations at different time scales. A planktonic foraminifera-based Sea Surface Temperature (SST) reconstruction is also provided, to have further insights on seasonal and annual temperature variations. In addition, spectral and wavelet analyses of the coccolithophore accumulation rates are performed to identify the different periodicities of coccolithophore productivity fluctuations. The study also benefits from the comparison with additional inorganic and organic geochemical proxies (Jiménez-Amat and Zahn, 2015; Martrat et al., 2014) and pollen data (Combourieu-Nebout et al., 2009) available at the same site, improving the paleoclimate reconstruction through a direct multi-proxy approach.

Area of Study

Present hydrographical conditions

The ODP Site 976 was recovered off the Spanish coast in the Alboran Sea, the westernmost basin of the Mediterranean Sea, bordering the Atlantic Ocean (Fig. 1). Surrounding lands include the high physiography of the Betic cordillera and Moroccan Rif mountains, that might provide a certain riverine input, although subjected to high seasonality and extreme climatic events (Jimenez-Espejo et al., 2008; Liquete et al., 2005; Lobo et al., 2006). Surface Atlantic Water (AW) pours inside the Alboran basin through the Strait of Gibraltar, as a constant stream of surface low-salinity waters called the Atlantic Jet (AJ). The latter contributes to the creation of two quasi-permanent meso-scale anticyclonic gyres: the Western Anticyclonic Gyre (WAG) and the Eastern Anticyclonic Gyre (EAG) (Fig. 1) (Heburn and La Violette, 1990; Sarhan et al., 2000). In the area, two mechanisms are known to be relevant for the upwelling dynamic: the southward drifting of the AJ, that would allow the water from below to rise, and the wind stress (Sarhan et al., 2000). The influence of the vertical mixing of AJ and deeper Mediterranean waters, concurrently with the complex bottom topography, forms areas of geostrophic front and quasi-permanent upwelling: the Alboran front and the Almeria-Oran front (Fig.1) (Perkins et al., 1990; Viúdez et al., 1996).

The combination of gyres and upwelling fronts results in increased nutrient availability and high productivity waters, among the richest within the rest of the Mediterranean (D'Ortenzio and D'Alcalà, 2009; Garcia-Gorriz and Carr, 1999). Counteracting the AW inflow, the denser and more saline Mediterranean waters exit the basin through the Mediterranean Outflow Water (MOW), that includes the western Mediterranean Deep Water (WMDW) from the Gulf of Lion and the Levantine Intermediate Water (LIW) from the far East of the Mediterranean basin (Fig. 1) (Millot, 2008; Perkins et al., 1990). Deep water formation is controlled by surface heat loss due to winds blowing from the north and north-west (Font et al., 2007; Mertens and Schott, 1998; Rixen et al., 2005; Smith et al., 2008).

Present Climate Conditions

The Alboran Sea climate conditions are under the influence of the Azores high pressure cell and its seasonal latitudinal shift, resulting in mild wet winters and dry hot summers (Lionello, 2012; Moreno et al., 2012; Rohling et al., 2015; Sumner et al., 2001). At decadal and inter-annual time scales, atmospheric variability is regulated by the North Atlantic Oscillation (NAO) index, which is characterized by positive (NAO+) and negative (NAO-) regimes (Hurrell, 1995; Olsen et al., 2012; Smith et al., 2016; Trigo et al., 2004). During a NAO+ regime, stronger pressure difference between the Azores High and Icelandic Low atmospheric cells brings storm trajectories to the north, determining stormier and wetter weather in northwest Europe and dryer winters in southern Europe and North Africa (Olsen et al., 2012; Smith et al., 2016; Zielhofer et al., 2017). At NAO- regime, weaker difference between the two pressure cells leads storm tracks to the south, enhancing precipitations over southern Europe and North Africa (Smith et al., 2016; Wanner et al., 2015). In the Iberian Peninsula, winter precipitation mode has been related to air masses raised by atmospheric instabilities and moisture supply from the tropical-subtropical North Atlantic corridor (Gimeno et al., 2010).

Materials and Methods

Core material and available data sets

The ODP Site 976 (Comas et al., 1996) is located about 60 km south of the Iberian Peninsula and about 110 km East of the Strait of Gibraltar (36°12.3′ N, 4°18.7′ W) (Fig. 1). The cores were recovered on the lower part of a very gentle slope, dipping southward of the Spanish margin in the Alboran Basin, at a depth of 1108 m. The investigated sediments are from Hole C – Core 1H – sections 1-3 (Comas et al., 1996), between 0.07 to 4.03 m below the sea floor. Main lithology is composed of nannofossil rich clay, with slight to moderate bioturbation and common shell fragments (Comas et

al., 1996). One Organic Rich Layer (ORL) occurs in the studied interval and is identified on the basis of the maximum accumulation of di- and tri- alkenones of 37 carbons (Martrat et al., 2004, 2014). The age model used in the present study is from Martrat et al. (2014), based on available ^{14}C calibrated AMS radiocarbon dates (Combourieu-Nebout et al., 2002, 2009). Sampling resolution of calcareous plankton dataset varies between 1 sample every 2 to 6 cm, according to the variable sedimentation rate (20 to 60 cm), thus providing a temporal resolution of one sample every ca. 100 years.

Calcareous plankton

The coccolith assemblages were analyzed in 129 samples. Sample preparation for the coccolith analysis follows the random settling technique by Flores and Sierro (1997). The quantitative analyses were performed using a polarized light microscopy at 1000X magnification. The relative abundance of taxa was estimated counting at least 500 specimens per sample, in variable fields of view. Reworked calcareous nannofossils were estimated separately during this counting. The absolute abundance of taxa is expressed as Nannofossil Accumulation Rate (NAR). The total NAR, used to determine coccolithophore paleoproductivity (Baumann et al., 2004; Steinmetz, 1994), was estimated following Flores and Sierro (1997):

$$\mathbf{NAR = N * w * S}$$

where **N** is the number of coccoliths per gram of sediment (Ng^{-1}), **w** is the wet bulk density ($g \times cm^{-3}$) (shipboard bulk density data, Comas et al., 1996), and **S** is the sedimentation rate ($cm \times ky^{-1}$). Wet bulk density is frequently used as a substitute to dry bulk density, in the absence of the latter, to estimate coccolithophore production (Grelaud et al., 2009; Marino et al., 2014; Stolz and Baumann, 2010). For taxonomic identification we referred to Young et al. (2003) and Jordan et al. (2004). According to Flores et al. (2000): gephyrocapsids with high angle bridge (>50°) and >3 μm in size are indicated as *Gephyrocapsa oceanica*; gephyrocapsids >3 μm in size with a low angle bridge (< 25°) are indicated as *Gephyrocapsa muellerae*; small *Gephyrocapsa* includes gephyrocapsids < 3μm in size. Specimens of *Emiliania huxleyi* were differentiated into two main groups following size criteria (Colmenero-Hidalgo et al., 2002): large *E. huxleyi* > 4 μm and small *E. huxleyi* < 4 μm. Warm water taxa are grouped according to their ecological preference for tropical-subtropical waters (Baumann et al., 2004; Boeckel and Baumann, 2004; Winter and Siesser, 1994). The group includes: *Calciosolenia* spp., *Discosphaera tubifera, Rhabdosphaera stylifera, Rhabdosphaera clavigera, Umbilicosphaera foliosa, Umbilicosphaera sibogae*, *Umbellosphaera* spp., *Oolithotus* spp.

Planktonic foraminifera assemblages were analyzed in 122 samples washed through 63 and 150μm sieves. The residues (>150μm) were split, until a representative aliquot containing about 300 specimens has been obtained. All specimens were counted in the aliquots and species abundances

were quantified as percentages on the total number of planktonic foraminifers (relative abundance) and as absolute abundances expressed as planktonic foraminifera Accumulation Rates (pfAR). The pfAR has been calculated following Giraudeau et al. (2001):

$$\mathbf{pfAR = AA * w * S}$$

where **AA** is the number of specimens per gram of dry sediment (nr/g), **w** is the wet bulk density ($g \times cm^{-3}$) (shipboard bulk density data, Comas et al., 1996), and **S** is the sedimentation rate ($cm \times ky^{-1}$). Sixteen species or species groups were distinguished. *Globigerinoides ruber* includes morphotypes of *G. ruber* white, and *Globigerinoides elongatus* (sensu Aurahs et al., 2011); *Trilobatus sacculifer* includes *Trilobatus trilobus*, *Trilobatus sacculifer* and *Trilobatus quadrilobatus* (sensu André et al., 2012; Hemleben et al., 1989; Spezzaferri et al., 2015). *Globoturborotalita rubescens* includes *Globoturborotalita tenella* because of their similar ecological preference (Capotondi et al., 1999). The taxonomy of *Neogloboquadrina* spp. follows criteria by Darling et al., (2006): *Neogloboquadrina incompta* includes specimens previously referred to *N. pachyderma* (dextral) and intergrades between *N. pachyderma* (dextral) and *N. dutertrei*. *Neogloboquadrina pachyderma* only includes the left coiling specimens.

According to their ecological preference (Hemleben et al., 1985; Kucera et al., 2005; Pujol and Vergnaud-Grazzini, 1995) and to previous Mediterranean Sea paleoclimatic reconstructions (De Rijk et al., 1999; Rohling et al., 1997), *G. ruber*, *T. sacculifer*, *Hastigerina pelagica*, *G. rubescens*, *Orbulina universa*, *Beella digitata* and *Globigerinella siphonifera* have been grouped as warm water taxa.

Sea Surface Temperature estimation

Planktic foraminifera assemblages were used to reconstruct annual, summer (July to September) and winter (January to March) SST with the modern analog technique non distance-weighted SIMMAX 28 and 10 analogs (Pflaumann et al., 1996). Considering that the study site is influenced by Atlantic and Mediterranean ocean circulation, following Schirrmacher et al. (2019), we use the combined North Atlantic core-top database (Kucera et al., 2005; Salgueiro et al., 2010, 2014) and the Mediterranean database (Hayes et al., 2005), and the root mean square error of both annual and seasonal SST reconstructions is about 1.3ºC (Schirrmacher et al., 2019).

Power spectral and wavelet analysis

Spectral and wavelet analyses were performed on the total NAR, displaying relevant high frequency oscillations throughout the record. The analysis of the non-stationary (frequency changes along time) and non-linear signals, was performed by applying the Empirical Mode Decomposition algorithm

(EMD) of Huang et al. (1998) in order to decompose multi-component signals into a series of amplitude and frequency modulation (AM-FM) waves, each with slowly varying amplitude and phase. A major advantage of EMD is that the basis functions are derived from the signal itself, hence the analysis is adaptive, in contrast to the traditional methods where the basis functions are fixed as sine and cosine for Fourier transform like methods and the mother wavelet functions for wavelet analysis.

The signal and the Intrinsic Mode Functions (IMF) components are analysed without interpolation, keeping the original evenly sampling intervals, with:

1. "REDFIT", that computes the spectrum of a possibly unevenly sampled time-series, by using the Lomb-Scargle Fourier transform. The spectrum is bias-corrected using spectra computed from simulated AR(1) series and the theoretical AR(1) spectrum (Lomb, 1976; Scargle, 1982; Schulz and Mudelsee, 2002).
2. Foster's (1996) weighted wavelet Z-transform (WWZ). To analyze non-stationary and irregularly sampled signals, we need an extension of the classic wavelet formalism. Foster (1996), who defines the WWZ, developed such extension as a suitable weighted projection method re-orthogonalizing the three basic functions (real and imaginary part of the Morlet wavelet and a constant) by rotating the matrix of their scalar products. Furthermore, he introduces statistical F-tests to distinguish between periodic components and a noisy background signal.

Results

Calcareous nannofossils

Calcareous nannofossils are generally abundant and well preserved and dissolution phenomena seem not to be significant. Abundances of the most relevant taxa are presented in Fig. 2 and no major discrepancies are observed between relative and absolute trends. The total NAR ranges between 0.5 x 10^{11} coccoliths x cm^{-2} x kyr^{-1} and 2 x 10^{11} coccoliths x cm^{-2} x kyr^{-1}, with an average of 0.8 x 10^{11} coccoliths x cm^{-2} x kyr^{-1}(Fig. 2). A marked abundance peak occurs at about 8.2 ka, and an oscillating pattern is recorded in the last 8 kyr (Fig. 2). Considering the relative abundances of the taxa (%), *E. huxleyi* < 4 μm represents the main taxon, having percentages between 40 and 60% and the highest values between 10 and 8 ka (Fig. 2). Among gephyrocapsids, *G. muellerae* results to be the most abundant in the lower part of the record, with values reaching 30% of the assemblage, followed by a descending trend (Fig. 2). Small *Gephyrocapsa* show an increase in abundance from 8%, between 10 and 7 ka, to 15% from 5.3 ka upward (Fig. 2). *Gephyrocapsa oceanica,* mainly represented by morphotypes larger than 5 μm, shows abundance fluctuations between 3 and 10% throughout the

Holocene (Fig. 2). *Florisphaera profunda*, although not a dominant component of the assemblages (with very few isolated peaks greater than 15%), shows a distinct pattern, with very low percentage values up to ~8 ka, that clearly increase upwards in fluctuating abundances (Fig. 2). Among less abundant taxa, *Syracosphaera* spp. (*S. histrica* and *S. pulchra*), having a mean value of 1%, show a distinct increase between 11 and 8 ka, reaching values of about 5% (Fig. 2). The warm water coccolith taxa have very low abundances throughout the succession, with a mean value of 2%; the group shows a gradual increase between 12 and 8 ka, and fluctuating pattern afterwards (Fig. 2). *Helicosphaera carteri* and *E. huxleyi* > 4 μm show a similar pattern with abundance values ranging between 10 and 15% in the lowest part of the succession (during the Younger Dryas), followed by a clear decreasing trend, with values around 1% (Fig. 2). Other taxa, not showing particular trends or significant fluctuations, are represented by *Coccolithus pelagicus* ssp. *pelagicus*, *Gephyrocapsa caribbeanica* and *Coronosphaera* spp., with percentages not higher than 5%. Subordinate taxa do not exceed the 3% of the assemblage and include *Coccolithus pelagicus* ssp. *braarudii*, *Coccolithus pelagicus* ssp. *azorinus*, *Braarudosphaera bigelowii*, *Calcidiscus leptoporus* ssp. small (3–5 μm), *C. leptoporus* ssp. *leptoporus* (5–8 μm), *C. leptoporus* ssp. *quadriperforatus* (8–10 μm), *Ceratolithus* spp., *Helicosphaera pavimentum*, *Helicosphaera hyalina*, *Pontosphaera* spp., *Gladiolithus flabellatus, Scyphosphaera* spp. and *Umbilicosphaera hulburtiana.* Reworked taxa occur in the samples with variable abundances, never exceeding about 4% (Fig. 2).

Planktonic foraminifera assemblages

Planktonic foraminifera are well preserved and diversified. Relative and absolute abundances of the most abundant/significant planktonic foraminifera taxa/ groups show comparable trends throughout the entire succession. *Neogloboquadrina incompta* and *Turborotalita quinqueloba* are abundant in the lower part of the record (between 12.5 ka and about 8 ka) and undergone a strong decreasing upward (Fig. 3). Although with lower relative and absolute abundances, *G. ruber* and *G. bulloides* are also abundant in this interval (Fig. 3). At about 8 ka, a prominent replacement of *G. inflata* at the expense of *N. incompta* and *T. quinqueloba* occurs. Starting from 8 ka upwards, *G. inflata* together with *G. bulloides* and *G. ruber*, became the most abundant taxon in the record (Fig. 3). *Globigerinita glutinata*, with relative abundances not higher than 10%, doesn't show any relevant fluctuation in the distribution pattern (Fig. 3). *Trilobatus sacculifer* became more abundant from about 8 ka upward, showing a more prominent increase, as relative and absolute abundances, during the last 3.5 kyr (Fig. 3). A similar distribution pattern is also shown by *Truncorotalita truncatulinoides* (Fig. 3). Other taxa showing a very scattered distribution in the studied interval, with relative abundances < 3 % and any

significant fluctuations, are not shown in Fig. 3. They are represented by *Globorotalia scitula*, *Globigerina falconensis*, *G. rubescens*, *N. pachyderma*, *G. siphonifera* and *O. universa*.

Sea Surface Temperature

Annual, summer and winter SST patterns show sharp fluctuations between 10.2 ka and 8.7 ka characterized by strong drops of winter and summer temperature values greater than 10°C (Fig. 3). During this interval an important increase of *T. quinqueloba* is observed, together with high occurrence of *N. incompta* and *N. dutertrei* and increasing trend of warm water foraminifera taxa (Fig. 5). In this interval, the similarity index slightly decreases (Fig. 3), indicating that this species combination is not usual in the modern oceanographic condition for the North Atlantic and the Mediterranean region. In this interval the average annual SST is about 13.9°C, while average winter and summer temperatures are 11.7°C and 16.7°C respectively (Fig. 3). For the last 8 kyr, the average annual SST is about 18.5°C, while winter SST in the Alboran Sea varies around ca. 15 °C, in agreement with modern conditions (15.4 °C; Locarnini et al., 2013) (Fig. 3). The average summer SST is 22.6°C, exceeding modern ones (21.4°C; Locarnini et al., 2013) (Fig. 3). Low temperatures values are recorded between about 8.6 and 7.7 ka both in summer (ca. 20°C) and in winter (ca.13°C) (Fig. 3). The highest temperatures are recorded between 7.7 ka and 5.8 ka with temperatures up to 23 °C during summer and up to 16 °C during winter (Fig. 3). During the last 5 kyr, summer SST weakly decreases, with slightly oscillating values between 22°C and 23°C (Fig. 3). In the same interval, winter SSTs are almost stable with average values of about 15°C (Fig. 3), although during the last 3 kyr, the winter temperatures are characterized by a slight increase.

These results suggest that, with the exception of the interval between 10.2 and 8.7 ka, our SST record shows values comparable with those derived from the alkenone-SST at the same site (Martrat et al., 2014), with the foram-based SST from other nearly records (Pérez-Folgado et al., 2003; Schirrmacher et al., 2019), and with the present-day SST in the region (Locarnini et al., 2013). On the basis of these considerations, only the last 8.6 kyr record has been considered for the climate interpretation.

Power spectral and wavelet analysis

The power spectrum of total NAR shows prominent peaks (over the 95% Confidence Level – C.L.) of periodicity ranging between 1100 yr and 1700 yr (IMF3) (Fig. 4a, c). The wavelet analysis reveals that periodicities are not evenly distributed through time and specifically the 1102 yr cycle occurs from 12 ka to about 4 ka (Fig. 4c), while the 1693 yr periodicity emerges since about 5 ka upwards (Fig. 4c). Significant peaks (over the 95% of C.L.) are observed at the periods of ~ 4300 yr and ~

8000 yr all along the record (IMF 4, 5) (Fig. 4 d,e). Scattered distribution of cycles between ~ 400 and ~ 700 yr are also observed (IMF 2) (Fig. 4b).

Discussion

Main hydrographic and climate variations

Surface water modifications occurring in the last 11 ka can be described by three main long-term (between 3-5000 c.a. years-long) steps: Phase I, II and III (Figs. 5-6).

Phase I – the early Holocene humid period

This phase straddles the early Holocene, between 11.5 ka and 8 ka and is subsequent to the Younger Dryas Stadial. The climate evolution of the latter stadial has been discussed in detail in Bazzicalupo et al. (2018) based on the same proxies and therefore not discussed in the present study. Phase I is marked by a gradual surface water temperature increase, well described by progressively growing abundances of both coccolithophore and foraminifera warm-water taxa, associated with increasing summer insolation (Fig. 5). During this phase, the distinct increase in both *Syrocosphaera* spp. and *T. quinqueloba* (Fig. 5) provides evidences of enhanced riverine/detrital input in surface waters. *Syracosphaera* spp. has been, in fact, related to enhanced supply of fresher and turbid upper layer (Ausín, et al., 2015b; Bazzicalupo et al., 2018; Colmenero-Hidalgo et al., 2004; Weaver and Pujol, 1988), while the cold taxon *T. quinqueloba* flourishes in high fertile and low density surface waters (Aksu et al., 2002; Hemleben et al., 1985; Pujol and Vergnaud-Grazzini, 1995; Triantaphyllou et al., 2010). Enhanced abundances of this taxon have been also related to areas influenced by continental runoff (Bartels-Jónsdóttir et al., 2015; Girone et al., 2013; Jonkers et al., 2010; Margaritelli et al., 2016; Rohling et al., 1997; Vallefuoco et al., 2012) and, in the Eastern Mediterranean, the increase in abundance of *T. quinqueloba*, during the deposition of sapropel layer S1, has been linked to a high tolerance for low salinity and highly stratified water conditions coupled with the presence of high nutrients and terrestrial organic material (Capotondi et al., 2004; Kontakiotis, 2016; Principato et al., 2006; Rohling et al., 1997; Zachariasse et al., 1997). The high abundance of small *Gephyrocapsa* during phase I (Fig. 6), also sustains nutrient availability in surface water (Gartner et al., 1987; Hernández-Almeida et al., 2011; Okada and Wells, 1997; Takahashi and Okada, 2000). A concomitant expansion of *Quercus* during phase I (Fig. 5) highlights enhanced humidity on land (Combourieu-Nebout et al., 2009) likely in relation with extreme seasonality during precession minima/insolation maxima (Fig. 5) and increased autumn/winter westerlies-carried rains over the western Mediterranean, which supports enhanced supply of fresher water into the basin. This scenario seems to reflect a regional climate condition since it is consistent with the establishment of the Early

Holocene humid phase, occurring between 11.5 and 7 ka (Jalut et al., 2009; Magny et al., 2002, 2013; Peyron et al., 2017; Zanchetta et al., 2007; Zielhofer et al., 2017) and with additional evidences of autumn/winter precipitation increase over the northern Mediterranean borderlands during northern Hemisphere insolation maxima (Kutzbach et al., 2013; Meijer and Tuenter, 2007; Toucanne et al., 2015; Tzedakis, 2007). Phase I is within the interval of sapropel layer S1 deposition in the Eastern Mediterranean (10.8-6.1 ka, De Lange et al., 2008), developed during maximum summer insolation, that contributed, through the enhanced monsoon precipitation, to increased runoff in the Eastern Mediterranean (Howell and Thunell, 1992; Rohling et al., 2002, 2004, 2015; Rossignol-Strick, 1985; Rossignol-Strick et al., 1982). Our data evidence that freshwater runoff during sapropel events was not restricted to the Eastern Mediterranean but was rather widespread over the entire Mediterranean Sea due to increased rainfall (Bard et al., 2002; Kallel et al., 2000; Kallel and Labeyrie, 1997; Toucanne et al., 2015; Zanchetta et al., 2007), thus strengthening the connection between North African summer monsoon and the increased western Mediterranean autumn/winter precipitation during sapropel deposition (Toucanne et al., 2015). On the other hand, phase I straddles the final phase of the deposition of ORL 1 as indicated by the decreasing, albeit still high, values of C_{37} (Fig. 5), and reduced deep water ventilation in the western Mediterranean (Frigola et al., 2007). Given the time offset between the beginning of the ORL1 formation (14.5 ka, Martrat et al., 2014), and the recorded enhanced riverine input and humidity on land at c.a. 11.5 ka, it appears unlikely that excess precipitation was the driving force of the ORL1 formation in the western Mediterranean (Rogerson et al., 2008). As stated in Bazzicalupo et al. (2018), shoaling of the nutricline and increased export production at the sea floor are relevant mechanism in the ORL1 deposition at the study core.

The 8.2 ka event

The transition between phase I and the following phase II is characterized by higher absolute abundances of *N. incompta* between ~8.6 ka and ~8.1 ka (Fig. 6) and by a sharp warm water taxa decrease (Fig. 5), suggesting water cooling. In more detail, a sharp and brief cooling event of about 3°C is recorded in annual, winter and summer SST (Fig. 6). An interruption of the surface water warming trend is also indicated by a decrease of warm water coccolith taxa in the early stage (Fig. 5). A concomitant temperate forest regression (Fig. 6) marks a short-term precipitation decrease episode.

This cooling episode is here related to the well-known cold and dry 8.2 ka event that punctuates the early Holocene evolution and it is broadly recognized in Greenland ice core records (Alley and Ágústsdóttir, 2005; Bond et al., 1997, 2001; Dansgaard et al., 1993; Lowe et al., 2008; Rasmussen et al., 2006; Rohling and Pälike, 2005) and in the Mediterranean (e.g. De Rijk et al., 1999; Lirer et al.,

2013; Rohling et al., 2002; Sprovieri et al., 2003). In the ODP Site 976, the modification of the water column structure indicated by calcareous plankton can be related to a southward displacement of the ITCZ (Intertropical Convergence Zone) and an intensified impact of harsher, higher-latitude climate conditions in the Mediterranean region (Rohling et al., 2002, 2004). Today, *N. incompta* does not dwell in the Alboran Sea due to the occurrence of deep pycnocline and nutricline (located at a depth of about 150-200m) and winter temperatures reaching 15°C (Pujol and Vergnaud Grazzini, 1995; Rohling et al., 1995). On the other hand, this taxon is abundant in the Gulf of Lion where strong winter mixing facilitates the advection of nutrients into the euphotic zone and, mainly, winter temperatures reach 12°C (Pujol and Vergnaud-Grazzini, 1995; Rohling et al., 1995).

The marked increase of coccolithophore production within the upper part of the 8.2 ka event, as indicated by the peak in total NAR (Fig. 2), is likely the result of an important hydrographic modification occurring at this time, related to the enhanced Atlantic water inflow. This feature marks the onset of the following phase II as discussed below and is very well comparable with a similar peak in the coccolithophore absolute abundance at 8.2 ka recorded in the Alboran Sea by Colmenero-Hidalgo et al. (2004) and related to the onset of gyre circulation into the basin.

Phase II: the middle Holocene establishment of the modern oceanographic circulation

Phase II represents the second major step in the hydrographic evolution of the basin. It develops between 8.2 ka and about 5.3 ka, thus it nearly represents the middle Holocene portion of the record (Bárcena et al., 2004; Giraudeau, 1993). It is marked by a distinct abundance increase of *F. profunda* and a subsequent increase of *G. inflata* (Fig. 6) which replaces *N. incompta*. *Florisphaera profunda* is a deep photic zone dweller and thrives with a deep nutricline and water column stratification (Baumann et al., 2005; Incarbona et al., 2013; Sprovieri et al., 2012), while *G. inflata* is a deep living taxon and benefits from water column stability, a deep pycnocline and reduced upwelling conditions. The shift between *G. inflata* and *N. incompta* is in agreement with Rohling et al. (1995) that linked this event to the establishment of the modern front-dominated conditions in the Alboran Sea, when the amount of Atlantic water inflow was close to the present volume. At Site 976, the enhanced Atlantic inflow, following the deglaciation and the sea level rise, would have deepened the nutricline favoring *F. profunda*. In addition, it would have promoted both the development of the modern geostrophic front, where *G. inflata* proliferates (Pujol and Vergnaud-Grazzini,1995; Rohling et al., 1995) and the establishment of WAG (Ausín et al., 2015b; Pérez-Folgado et al., 2003; Rohling et al., 1995). This hydrographic evolution follows the culmination of the highest rate of global sea-level rise (Lambeck et al., 2014). Concurrently to the development of a deep nutricline, high annual and seasonal SSTs are recorded (Fig. 6) also marked by the increase of the tropical taxon *T. sacculifer*

(Fig. 6). Conversely, small *Gephyrocapsa* and neogloboquadrinids decrease (Fig. 6). We suggest that anomalous sea-surface warmer conditions during this period promoted a prolonged water column stratification, deepening of the thermocline (nutricline) and decrease of winter wind-induced mixing. These conditions contributed to a higher increase of warm and oligotrophic taxa, that currently thrives during mid-summer in the Mediterranean Sea (Bárcena et al., 2004; Pujol and Vergnaud-Grazzini, 1995), and decreasing of those taxa more related to nutrient-rich conditions such as small *Gephyrocapsa* and neogloboquadrinids. The occurrence of *G. bulloides* during this phase (Fig. 6) is consistent with its opportunistic behavior (Pujol and Vergnaud-Grazzini, 1995; Rohling et al., 1997; Schiebel et al., 2001) and its favorite habitat, highly dependent on enhanced food availability, related to strong seasonal contrast or river input. High abundances of temperate forest in the early stage of phase II (Fig. 6) suggest still wet climate conditions on land. This phase, although coeval with the younger portion of S1, is subsequent to the end of ORL 1 deposition in the Alboran Sea (Fig. 5). Deep anoxia in the western basin is in fact independent of that of the eastern basin (Rogerson et al., 2008) and ORL 1 termination is related to the 8.2 ka event and to the establishment of the modern front-dominated conditions in the western Mediterranean (Cacho et al., 2002; Rogerson et al., 2008). During phase II, differently from phase I occurring during ORL1 deposition and characterized by shoaling of the nutricline and enhanced productivity in surface water (Bazzicalupo et al., 2018), the calcareous plankton assemblages indicate stratified conditions in column water and deep nutricline, which likely prevented productivity in surface water and export production at the sea floor. This datum supports the hypothesis that productivity, although does not represent the triggering mechanism, may provide a secondary control in the ORL formation (Rogerson et al., 2008).

Phase III: the late Holocene reduced seasonality

This phase is marked by the coeval increase of small *Gephyrocapsa* and *G. bulloides*, at c.a. 5.3 ka (Fig. 6), suggesting increased nutrient availability in surface waters. These taxa are, in fact, considered high surface water productivity proxies (Barcena et al., 2004; Colmenero-Hidalgo et al., 2004; Gartner et al., 1987; Pujol and Vergnaud-Grazzini, 1995 Takahashi and Okada, 2000). The enhanced abundances of the deep mixed dweller *T. truncatulinoides* (Fig. 6) support more intense seasonal and prolonged mixing. Elevated abundances of *T. truncatulinodes* from sediment trap in the Gulf of Lions have been related to increased winter mixing conditions (Rigual-Hernández et al., 2012). On the other hand, the high abundance of *F. profunda* and *G. inflata* (Fig. 6) is still in relation with the modern front-dominated conditions in the Alboran Sea and deep nutricline, originating at the onset of phase II. Oscillations in the absolute abundances of *F. profunda* as well as of small *Gephyrocapsa* (Fig. 6) are likely in relation with short-term fluctuations in total NAR, which are

441 discussed in more detail below. Foraminifera warm-water taxa, together with G. *ruber* group and to
442 a less degree warm water coccolith taxa, show a general decreasing trend (Fig. 5). The summer SST
443 record (Fig. 6) is in line with reducing summer insolation trend (Fig. 5) and with evidence from the
444 western Mediterranean terrestrial record of reduced seasonality (cooler summers and warmer winters)
445 during the transition to late Holocene (Ramos-Román et al., 2018). The aridification process,
446 accompanying the reduced seasonality at this time is highlighted, in the pollen record, by an increase
447 in *Artemisia* at around 4 ka at the studied core (Fig. 6), and by several coeval Mediterranean records
448 (Desprat et al., 2013; Fletcher et al., 2012; Fletcher and Sánchez Goñi, 2008; Jalali et al., 2016; Jalut
449 et al., 2000, 2009; Magny et al., 2013; Ramos-Román et al., 2018).
450 The last 3.5 kyr of phase III are marked by a relevant increase of *T. sacculifer* (Fig. 6). The distribution
451 pattern of this taxon is punctuated by three main short-term pulses (Ts1-Ts3 in Fig. 6), not previously
452 recorded in the western Mediterranean. *Trilobatus sacculifer* mainly occurs in warm and oligotrophic
453 tropical and sub-tropical waters with low seasonality (Bé and Hutson, 1977; Fraile et al., 2008;
454 Hemleben et al., 1989; Vincent and Berger, 1981). Today this taxon reaches its maximum abundance
455 in the Eastern Mediterranean basin and in the Red Sea, where low nutrient and warm surface waters
456 prevail throughout the year, due to the relatively stable deep pycnocline (Kallel and Labeyrie, 1997;
457 Kucera et al., 2005; Pujol and Vergnaud-Grazzini, 1995; Siccha et al., 2009). In the Red Sea, its
458 increasing trend, during the Holocene, has been also related to more arid conditions during reduced
459 monsoon climate system and prevailing eastern Mediterranean climate system (Edelman-Furstenberg
460 et al., 2009). In our record, the last 3.5 kyr are characterized by a reduction of seasonal thermal
461 gradient ($\Delta SST_{sum\text{-}win}$, Fig. 6) in the seawater, likely related to weak increase of winter SST,
462 concomitant with ameliorate climate condition on land, as suggested by coeval relative increases of
463 temperate forests in the pollen assemblages (Fig. 6). A positive correlation between *T. sacculifer* and
464 weaker winter conditions and stratification has been also found in the Arabian Sea (Munz et al.,
465 2015). We suggest that, at Site 976, relatively higher winter SSTs (with values exceeding 15°C) with
466 respect to the earlier interval, developed more stable year-round surface water conditions in the basin
467 favoring the increase of *T. sacculifer* in the last 3.5 kyr. Such conditions could probably represent the
468 response to changes in hydrological conditions in the adjacent Iberian basin, related to the reduction
469 of meltwater discharge in the North Atlantic (Bond et al., 2001). In the Gulf of Cádiz, according to
470 Schirrmacher et al. (2019), larger seasonal SST contrasts, during the Holocene, are related to periods
471 of enhanced iceberg discharge; the northward heat transport was blocked due to freshwater forcing
472 in the North Atlantic resulting in colder winter temperatures and higher summer temperatures due to
473 a seasonal northward migration of Intertropical Convergence Zone (ITCZ). This mechanism is similar
474 to the one proposed by Repschläger et al. (2017) for the early Holocene, when reinforcements of

475 northward heat transport and migration of Subtropical Gyre is found during periods of weak north
476 Atlantic meltwater discharge. Similarly, we retain that the decrease in the drift ice index during the
477 last 3 kyr (Bond et al., 2001), could have promoted higher northward advection of warmer water
478 masses that could have also reached the Alboran Sea through the Strait of Gibraltar, favoring the
479 instauration of a lower seasonal thermal gradient. The three distinct peaks of *T. sacculifer*, centered
480 at about 2.9 ka, 1.8 ka and 0.7 ka, trace the occurrence of short warm pulses at the core location. They
481 appear chronologically correlated with the short-term warm and dry events identified in northwestern
482 Africa lakes and in the Adriatic Sea (Piva et al., 2008; Zielhofer et al., 2017). The phase Ts1 is also
483 chronologically correlated with the warm phase recognized by Margaritelli et al. (2016) during the
484 Middle Bronze Age–Iron Age in the central Mediterranean.
485
486 *Millennial scale variations*
487 Since the WAG establishment in the Alboran Sea at ca. 8 ka, total NAR values show a series of
488 millennial-scale fluctuations over the middle and late Holocene at Site 976 (Fig. 7). This pattern
489 indicates that high-frequency variations in the coccolithophore productivity are superimposed to the
490 main climate phases. Connecting coccolithophore productivity to environmental proxies is a complex
491 task since multiple relationships might affect the link between the various signals. A certain
492 chronological uncertainty is also added, when comparing different sites with different age models. In
493 order to unravel the forcing mechanism responsible for coccolithophore productivity variations at the
494 studied core, we compared a few coccolithophore proxies with the pattern of $\delta^{18}O_{seawater}$ available at
495 the ODP Site 976 (Jiménez-Amat and Zahn, 2015), as a proxy of local surface water salinity variation.
496 We have also performed a comparison with the detrended $\delta^{18}O_{speleothem}$ curve (Smith et al., 2016),
497 which represents a high-resolution archive of quasi-cyclical events of relatively wet-to-dry climatic
498 conditions over Iberia, with a ~1500 year frequency (Smith et al., 2016). This trend is significantly
499 correlated with the NAO index (Olsen et al., 2012) (Fig. 7). A relationship between coccolithophore
500 productivity and NAO modes has been recently suggested in the Alboran Sea by Ausín et al. (2015a).
501 These authors indicate weakened (intensified) upwelling, related to weaker (stronger) westerlies,
502 responsible for reduced (reinforced) WMDW in the Gulf of Lions. In this scenario, the NAO
503 circulation mode is the forcing mechanism of coccolithophore variability. Intensified upwelling
504 would have been promoted by stronger westerlies blowing over the Gulf of Lions, during a NAO –
505 mode. These conditions would have promoted major WMDW formation and simultaneous
506 enhancement of the AJ influx, both fluctuating in-phase (Ausín et al., 2015a; García Lafuente et al.,
507 2002, 2007) . The AJ would have migrated southward, allowing the cool subsurface waters to fill the
508 area left behind the jet (Sarhan, 2000) and thus promoting upwelling. In the present work, a first

comparison between datasets indicates that low salinity phases (lighter $\delta^{18}O_{seawater}$) are concurrent with high values of *G. oceanica* (Fig. 7). The occurrence of *G. oceanica* within the western Mediterranean basin has been often related to Atlantic surface water inflows (Álvarez et al., 2010; Bárcena et al., 2004; Bazzicalupo et al., 2018; Knappertsbusch, 1993; Oviedo et al., 2017). The positive correlation of the coccolithophore taxon with salinity minima at Site 976, further supports the relation between *G. oceanica* and Atlantic surface water inflows, since salinity minimum in the Alboran Sea essentially traces phases of enhanced Atlantic water into the basin (Font et al., 1998; Sarhan et al., 2000; Viúdez et al., 1996). Consequently, we use the lighter values of $\delta^{18}O_{seawater}$ and the increased abundance of *G. oceanica* as proxies of Atlantic inflow in the Alboran Sea (Fig. 7), which both provide a regime of cyclical Atlantic water inflow intensity in the basin. Coccolithophore productivity variations, expressed as total NAR, display distinct pulses, well-correlated with the pattern of the changing Atlantic inflow intensity and with the concomitant occurrence of alternating dry/wet phases in the Iberia $\delta^{18}O_{speleothem}$ (Fig. 7). Therefore, the various proxies point out to a coupling between enhanced coccolithophore productivity (high total NAR values), intensified Atlantic waters inflow (lighter $\delta^{18}O_{seawater}$ and increased abundance of *G. oceanica*), and arid conditions over the Iberia Peninsula (peaks in $\delta^{18}O_{speleothem}$), correlated with NAO+ phases (Fig. 7). Our data support the model proposed by Ausín et al. (2015a), and specifically the relation between coccolithophore productivity, Atlantic inflow and WMDW strength, although the dataset at site 976 indicate an opposite relationship between coccolithophore productivity and NAO mode. According to the present results, enhanced Atlantic water inflow occurred during a persistent NAO+ index (Fig. 7); the latter would have strengthened the north-westerlies over the northwestern Mediterranean basin, promoting a reinforcement of deepwater overturning and in turn increased the AJ (Fig. 8). The suggested relation between NAO mode and WMDW strength is in agreement with results from today's survey in the western Mediterranean (Rixen et al., 2005) and with the proposed relationship between strengthening of the WMDW and NAO variability in the past. In fact, during the Holocene and the Dansgaard-Oeschger events NAO + phases would have strengthen the northwesterlies over the northwestern Mediterranean, enhancing the WMDW formation (Frigola et al., 2007; Moreno et al., 2002, 2004, 2005; Nieto-Moreno et al., 2011). The scenario is also consistent with the observed decadal-variability between NAO intensity and upwelling strength highlighted in the western Mediterranean (Vargas-Yáñez et al., 2008). A possible reasonable explanation for the differing interpretations between the present work and the Ausín et al. (2015a) study, is that the latter authors based their paleoceanographic reconstruction on oscillations of the *F. profunda* NAR abundances in the Alboran Sea. In Ausín et al. (2015a), *F. profunda* NAR peaks have been linked to the intensification of the upwelling conditions in the area. Recent data establish a precise relationship

between *F. profunda* and primary productivity levels in today's low-latitude oceans (Hernández-Almeida et al., 2019) and suggest that the link between *F. profunda* abundance and net primary productivity in the Mediterranean Sea is not straight forward thus discouraging the use of this taxon as a productivity indicator into the basin (Hernández-Almeida et al., 2019).

External and internal forcing mechanisms of coccolithophore productivity cycles

The time series analysis performed on the total NAR record confirms the occurrence of millennial-scale periodicities in coccolithophore productivity during the Holocene and highlights two main periodicities through the record: the first one of ~ 1100 yr (from 12.5 to c.a. 5 ka) and the second one of ~ 1700 yr (from 5 to 0.19 ka) (Fig. 4c). The results of spectral and wavelength analyses indicate that coccolithophore productivity changes in the Alboran Sea were modulated both by external (solar) and internal (oceanic-atmospheric) forcing. In fact, the ~ 1100 yr-cycles appear close to the ~ 1000 yr cycle identified during the early Holocene in solar proxies in North Atlantic records and in IRD record (Debret et al., 2007, 2009). They are also detected in the western Mediterranean pollen record, which displays a periodic component of ~ 900 yr (Fletcher et al., 2012) and of ~ 1100 yr (Ramos-Román et al., 2018) during the early and middle Holocene. On the other hand, cycles of ~ 1700 yr are very close to the 1600-year cycle dominating during the last 5000 yr in several paleoclimate records (Debret et al., 2007; 2009 and references therein) and related to internal (oceanic/atmospheric) forcing. A similar shift in periodicity to a dominant ~ 1750 oscillation in the last 6 ka (Fletcher et al., 2012) and ~ 1600 yr-cycle (Ramos-Román et al., 2018) in the last 4.7 ka has been detected in the western Mediterranean in the pollen record and is related to the influence of NAO-like circulation in the mid-late Holocene. The similar pattern in cyclicity observed in the present study in NAR pattern in the Alboran Sea strengthens the relation between coccolithophore productivity/hydrographic changes and atmospheric variability modulated by NAO fluctuations and sustains the occurrence of a periodicity change through the Holocene from a dominant external (solar) to a dominant internal (oceanic/atmospheric) forcing.

Conclusions

The calcareous plankton assemblage (coccolithophore and foraminifera) of the ODP Site 976 from the Alboran Sea has been studied at a centennial-scale resolution, to investigate the climate variability and the forcing mechanisms affecting the western Mediterranean basin during the last 12.5 ka. Coccolithophore and planktonic foraminifera dataset is integrated with pollen and geochemical data available at the site. During a first step, between 11.5 and 8.2 ka, calcareous plankton assemblage clearly traces increasing temperature and freshwater arrival, related to riverine input in the basin,

during a period of insolation maxima. The timing of this phase in the Alboran Sea is quasi concomitant with sapropel S1 deposition in the eastern Mediterranean, suggesting a connection between the monsoonal mechanism for sapropel formation and high rainfall conditions in Northwestern Europe. Following an abrupt surface water temperature decrease correlated with humidity reduction and centered at 8.2 ka, the second phase (8-4.6 ka) is marked by a profound change in the planktonic assemblages, reflecting a more stratified water column, the deepening of the nutricline following a sea level rise and the instauration of the modern gyre circulation. The third final phase (4.6-0.19 ka) is characterized by reduced seasonality (cooler summers and warmer winters), enhanced surface water mixing and increased aridification on land related with a decrease in summer insolation. Short-term cyclicity occurs in coccolithophore productivity, with a clear pattern mainly occurring since the establishment of the modern circulation. Millennial-cycles of increased coccolithophore productivity are associated with enhanced inflows of Atlantic water from the Gibraltar strait modulated by NAO+ mode. The proposed scenario strengthens the role of hydrographic changes and atmospheric variability modulated by NAO fluctuations on coccolithophore productivity in the Alboran Sea. The results of the spectral analysis add information on the value of coccolithophores in recording environmental changes and highlight that coccolithophore productivity is modulated by both external (solar) and internal (oceanic-atmospheric) forcing. A shift in periodicity from a dominant ~ 1100 yr oscillations to ~ 1600 yr periodicity occurs at about 4 ka and appears in agreement with enhanced influence of NAO-like circulation during the late Holocene.

Acknowledgements

Two anonymous reviewers are greatly acknowledged for their valuable contributions which improved the early version of this manuscript. The authors thank the Ocean Drilling Program for providing the samples of ODP Site 976. This research was financially supported by the Geoscience PhD scholarship, Università degli Studi di Bari, and benefited of instrumental upgrades from "Potenziamento Strutturale PONa3_00369 dell'Università degli Studi di Bari, Laboratorio per lo Sviluppo Integrato delle Scienze e delle Tecnologie dei Materiali Avanzati e per dispositivi innovativi (SISTEMA). E.S. was funded by a postdoctoral fellowship (SFRH/ BPD/111433/2015) from Fundação para a Ciência e a Tecnologia (FCT).

References

Aksu AE, Hiscott RN, Kaminski MA, et al. (2002) Last glacial–Holocene paleoceanography of the

611 Black Sea and Marmara Sea: stable isotopic, foraminiferal and coccolith evidence. *Marine*
612 *Geology* 190(1–2). Elsevier: 119–149. DOI: 10.1016/S0025-3227(02)00345-6.

613 Alley RB and Ágústsdóttir AM (2005) The 8k event: Cause and consequences of a major Holocene
614 abrupt climate change. *Quaternary Science Reviews* 24(10–11): 1123–1149. DOI:
615 10.1016/j.quascirev.2004.12.004.

616 Álvarez MC, Amore OF, Cros LL, et al. (2010) Coccolithophore biogeography in the
617 Mediterranean Iberian margin. *Revista Española de Micropaleontologia* 42(3): 359–371.

618 André A, Weiner A, Quillévéré F, et al. (2012) The cryptic and the apparent reversed: lack of
619 genetic differentiation within the morphologically diverse plexus of the planktonic foraminifer
620 Globigerinoides sacculifer. *Paleobiology* 39(01). GeoScienceWorld: 21–39. DOI:
621 10.1666/0094-8373-39.1.21.

622 Aurahs R, Treis Y, Darling K, et al. (2011) A revised taxonomic and phylogenetic concept for the
623 planktonic foraminifer species Globigerinoides ruber based on molecular and morphometric
624 evidence. *Marine Micropaleontology* 79(1–2). Elsevier: 1–14.

625 Ausín B, Flores JA, Sierro FJ, Cacho I, et al. (2015a) Atmospheric patterns driving Holocene
626 productivity in the Alboran Sea (Western Mediterranean): A multiproxy approach. *The*
627 *Holocene* 25(4): 583–595. DOI: 10.1177/0959683614565952.

628 Ausín B, Flores JA, Sierro FJ, Bárcena MA, et al. (2015b) Coccolithophore productivity and
629 surface water dynamics in the Alboran Sea during the last 25kyr. *Palaeogeography,*
630 *Palaeoclimatology, Palaeoecology* 418. Elsevier B.V.: 126–140. DOI:
631 10.1016/j.palaeo.2014.11.011.

632 Bárcena MA, Cacho I, Abrantes F, et al. (2001) Paleoproductivity variations related to climatic
633 conditions in the Alboran Sea (western Mediterranean) during the last glacial-interglacial
634 transition: The diatom record. *Palaeogeography, Palaeoclimatology, Palaeoecology* 167(3–4):
635 337–357. DOI: 10.1016/S0031-0182(00)00246-7.

636 Bárcena MA, Flores JA, Sierro FJ, et al. (2004) Planktonic response to main oceanographic changes
637 in the Alboran Sea (Western Mediterranean) as documented in sediment traps and surface
638 sediments. *Marine Micropaleontology* 53(3–4): 423–445. DOI:
639 10.1016/j.marmicro.2004.09.009.

640 Bard E, Delaygue G, Rostek F, et al. (2002) Hydrological conditions over the western
641 Mediterranean basin during the deposition of the cold Sapropel 6 (ca. 175 kyr BP). *Earth and*
642 *Planetary Science Letters* 202(2). Elsevier: 481–494. DOI: 10.1016/S0012-821X(02)00788-4.

643 Bartels-Jónsdóttir HB, Voelker AHL, Abrantes FG, et al. (2015) High-frequency surface water
644 changes in the Tagus prodelta off Lisbon, eastern North Atlantic, during the last two millennia.
645 *Marine Micropaleontology* 117. Elsevier: 13–24. DOI: 10.1016/J.MARMICRO.2015.03.001.

646 Baumann K-H, Boeckel B, Frenz M, et al. (2004) Coccolith contribution to South Atlantic
647 carbonate sedimentation; Coccolithophores; from molecular processes to global impact. In:
648 *Coccolithophores - From Molecular Processes to Global Impact*, pp. 367–402. DOI:
649 10.1016/S0079-6352(99)80122-2.

650 Baumann K-H, Andruleit H, Böckel B, et al. (2005) The significance of extant coccolithophores as
651 indicators of ocean water masses, surface water temperature, and palaeoproductivity: a review.
652 *Paläontologische Zeitschrift* 79(1): 93–112. DOI: 10.1007/BF03021756.

653 Bazzicalupo P, Maiorano P, Girone A, et al. (2018) High-frequency climate fluctuations over the
654 last deglaciation in the Alboran Sea, Western Mediterranean: Evidence from calcareous
655 plankton assemblages. *Palaeogeography, Palaeoclimatology, Palaeoecology* 506. Elsevier:
656 226–241. DOI: 10.1016/J.PALAEO.2018.06.042.

657 Bé AWH and Hutson WH (1977) Ecology of Planktonic Foraminifera and Biogeographic Patterns
658 of Life and Fossil Assemblages in the Indian Ocean. *Micropaleontology* 23(4). The
659 Micropaleontology Project., Inc.: 369. DOI: 10.2307/1485406.

660 Boeckel B and Baumann K-H (2004) Distribution of coccoliths in surface sediments of the south-
661 eastern South Atlantic Ocean: Ecology, preservation and carbonate contribution. *Marine*
662 *Micropaleontology* 51(3–4): 301–320. DOI: 10.1016/j.marmicro.2004.01.001.

663 Bond G, Showers W, Cheseby M, et al. (1997) A pervasive Millennial-scale cycle in the North
664 Atlantic Holocene Climate. *Science* 278: 1257–1266.

665 Bond G, Kromer B, Beer J, et al. (2001) Persistent solar influence on North Atlantic climate.
666 *Science* 294(5549): 2130–2136. DOI: 10.1126/science.1065668.

667 Cacho I, Grimalt JO, Pelejero C, et al. (1999) Dansgaard-Oeschger and Heinrich event imprints in
668 Alboran Sea paleotemperatures. *Paleoceanography* 14(6). John Wiley & Sons, Ltd: 698–705.

669 DOI: 10.1029/1999PA900044.

670 Cacho I, Grimalt JO, Canals M, et al. (2001) Variability of the western Mediterranean Sea surface
671 temperature during the last 25,000 years and its connection with the Northern Hemisphere
672 climatic change. *Paleoceanography* 16(1): 40–52. DOI: 10.1029/SP010.

673 Cacho I, Grimalt JO and Canals M (2002) Response of the Western Mediterranean Sea to rapid
674 climatic variability during the last 50,000 years: A molecular biomarker approach. *Journal of*
675 *Marine Systems* 33–34: 253–272. DOI: 10.1016/S0924-7963(02)00061-1.

676 Capotondi L, Maria Borsetti A and Morigi C (1999) Foraminiferal ecozones, a high resolution
677 proxy for the late Quaternary biochronology in the central Mediterranean Sea. *Marine Geology*
678 153(1–4). Elsevier: 253–274. DOI: 10.1016/S0025-3227(98)00079-6.

679 Capotondi L, Soroldoni E, Principato MS, et al. (2004) Late Quaternary planktonic foraminiferal
680 distributions : problems related to size fraction. *Proceedings of the First Italian Meeting on*
681 *Environmental Micropaleontology* (9): 1–6.

682 Català A, Cacho I, Frigola J, et al. (2018) Holocene hydrography evolution in the Alboran Sea: a
683 multi-record and multiproxy comparison. *Climate of the Past Discussions* 15(3): 927–942.

684 Cita MB, Vergnaud-Grazzini C, Robert C, et al. (1977) Paleoclimatic Record of a Long Deep Sea
685 Core from the Eastern Mediterranean. *Quaternary Research* 8(2). Cambridge University Press:
686 205–235. DOI: 10.1016/0033-5894(77)90046-1.

687 Colmenero-Hidalgo E, Flores JA and Sierro FJ (2002) Biometry of Emiliania huxleyi and its
688 biostratigraphic significance in the Eastern North Atlantic Ocean and Western Mediterranean
689 Sea in the last 20 000 years. *Marine Micropaleontology* 46(3–4): 247–263. DOI:
690 10.1016/S0377-8398(02)00065-8.

691 Colmenero-Hidalgo E, Flores JA, Sierro FJ, et al. (2004) Ocean surface water response to short-
692 term climate changes revealed by coccolithophores from the Gulf of Cadiz (NE Atlantic) and
693 Alboran Sea (W Mediterranean). *Palaeogeography, Palaeoclimatology, Palaeoecology* 205(3–
694 4): 317–336. DOI: 10.1016/j.palaeo.2003.12.014.

695 Comas M, Zahn R and Klaus A (1996) *Ocean Drilling Program LEG 161 Preliminary Report*
696 *Mediterranean Sea II - The Western Mediterranean*. *ODP Preliminary Report*.

697 Combourieu-Nebout N, Turon JL, Zahn R, et al. (2002) Enhanced aridity and atmospheric high-

pressure stability over the western Mediterranean during the North Atlantic cold events of the past 50 k.y. *Geology* 30(10): 863.

Combourieu-Nebout N, Peyron O, Dormoy I, et al. (2009) Rapid climatic variability in the west Mediterranean during the last 25 000 years from high resolution pollen data. *Climate of the Past* 5: 503–521. DOI: 10.1109/IGARSS.2010.5652499.

Corselli C, Principato MS, Maffioli P, et al. (2002) Changes in planktonic assemblages during sapropel S5 deposition: Evidence from Urania Basin area, eastern Mediterranean. *Paleoceanography* 17(3). DOI: 10.1029/2000PA000536.

D'Ortenzio F and D'Alcalà MR (2009) On the trophic regimes of the Mediterranean Sea: A satellite analysis. *Biogeosciences* 6(2): 139–148. DOI: 10.5194/bg-6-139-2009.

Dansgaard W, Johnsen SJ, Clausen HB, et al. (1993) Evidence for general instability of the past climate from a 250-kyr ice-core record. *Nature* 364: 218–220. DOI: 10.2307/1178566.

Darling KF, Kucera M, Kroon D, et al. (2006) A resolution for the coiling direction paradox in *Neogloboquadrina pachyderma*. *Paleoceanography* 21(2). John Wiley & Sons, Ltd: n/a-n/a. DOI: 10.1029/2005PA001189.

De Lange GJ, Thomson J, Reitz A, et al. (2008) Synchronous basin-wide formation and redox-controlled preservation of a Mediterranean sapropel. *Nature Geoscience* 1(9): 606–610. DOI: 10.1038/ngeo283.

De Rijk S, Troelstra SR and Rohling EJ (1999) Benthic foraminiferal distribution in the Mediterranean Sea. *The Journal of Foraminiferal Research* 29(2). GeoScienceWorld: 93–103. DOI: 10.2113/gsjfr.29.2.93.

Debret M, Bout-Roumazeilles V, Grousset F, et al. (2007) The origin of the 1500-year climate cycles in Holocene North-Atlantic records. Available at: https://hal-sde.archives-ouvertes.fr/hal-00330731/ (accessed 20 June 2019).

Debret M, Sebag D, Crosta X, et al. (2009) Evidence from wavelet analysis for a mid-Holocene transition in global climate forcing. *Quaternary Science Reviews* 28(25–26). Elsevier Ltd: 2675–2688. DOI: 10.1016/j.quascirev.2009.06.005.

Desprat S, Combourieu-Nebout N, Essallami L, et al. (2013) Deglacial and holocene vegetation and climatic changes in the southern central Mediterranean from a direct land-sea correlation.

727 *Climate of the Past* 9(2): 767–787. DOI: 10.5194/cp-9-767-2013.

728 Edelman-Furstenberg Y, Almogi-Labin A and Hemleben C (2009) Palaeoceanographic evolution of
729 the central Red Sea during the late Holocene. *Holocene* 19(1): 117–127. DOI:
730 10.1177/0959683608098955.

731 Fletcher WJ and Sánchez Goñi MF (2008) Orbital- and sub-orbital-scale climate impacts on
732 vegetation of the western Mediterranean basin over the last 48,000 yr. *Quaternary Research*
733 70(3): 451–464. DOI: 10.1016/j.yqres.2008.07.002.

734 Fletcher WJ, Debret M and Sanchez Goñi M (2012) The Holocene frequency millennial oscillation
735 in western Mediterranean climate: Implications for past dynamics of the North Atlantic
736 atmospheric westerlies. *The Holocene* 23(2): 153–166. DOI: 10.1177/0959683612460783.

737 Flores JA and Sierro FJ (1997) Revised technique for calculation of calcareous nannofossil
738 accumulation rates. *Micropaleontology* 43(3): 321–324. DOI: 10.2307/1485832.

739 Flores JA, Gersonde RR, Sierro FJ, et al. (2000) Southern ocean pleistocene calcareous nannofossil
740 events: Calibration with isotope and geomagnetic stratigraphies. *Marine Micropaleontology*
741 40(4): 377–402. DOI: 10.1016/S0377-8398(00)00047-5.

742 Font J, Millot C, Salas J, et al. (1998) The drift of Modified Atlantic Water from the Alboran Sea to
743 the eastern Mediterranean. *Scientia Marina* 62(3): 211–216. DOI:
744 10.3989/scimar.1998.62n3211.

745 Font J, Puig P, Salat J, et al. (2007) Sequence of hydrographic changes in NW Mediterranean deep
746 water due to the exceptional winter of 2005. *Scientia Marina* 71(2): 339–346. DOI:
747 10.3989/scimar.2007.71n2339.

748 Foster G (1996) Wavelets for period analysis of unevenly sampled time series. *Astron. J.* 112:
749 1709–1729.

750 Fraile I, Schulz M, Mulitza S, et al. (2008) Predicting the global distribution of planktonic
751 foraminifera using a dynamic ecosystem model. *Biogeosciences* 5: 891–911.

752 Frigola J, Moreno A, Cacho I, et al. (2007) Holocene climate variability in the western
753 Mediterranean region from a deepwater sediment record. *Paleoceanography* 22(2): 1–16. DOI:
754 10.1029/2006PA001307.

755 Frigola J, Moreno A, Cacho I, et al. (2008) Evidence of abrupt changes in Western Mediterranean
756 Deep Water circulation during the last 50 kyr: A high-resolution marine record from the
757 Balearic Sea. *Quaternary International* 181(1): 88–104. DOI: 10.1016/j.quaint.2007.06.016.

758 Garcia-Gorriz E and Carr M-E (1999) The climatological annual cycle of satellite-derived
759 phytoplankton pigments in the Alboran sea. *Geophysical Research Letters* 26(19): 2985–2988.

760 García Lafuente J, Fanjul EÁ, Vargas JM, et al. (2002) Subinertial variability in the flow through
761 the Strait of Gibraltar. *Journal of Geophysical Research* 107(C10). John Wiley & Sons, Ltd:
762 3168. DOI: 10.1029/2001JC001104.

763 García Lafuente J, Sánchez Román A, Díaz del Río G, et al. (2007) Recent observations of seasonal
764 variability of the Mediterranean outflow in the Strait of Gibraltar. *Journal of Geophysical*
765 *Research* 112(C10). John Wiley & Sons, Ltd: C10005. DOI: 10.1029/2006JC003992.

766 Gartner S, Chow J and Stanton RJ (1987) Late Neogene paleoceanography of the Eastern
767 Caribbean, the Gulf of Mexico, and the Eastern Equatorial Pacific. *Marine Micropaleontology*
768 12: 255–304.

769 Gimeno L, Nieto R, Trigo RM, et al. (2010) Where Does the Iberian Peninsula Moisture Come
770 From? An Answer Based on a Lagrangian Approach. *Journal of Hydrometeorology* 11(2):
771 421–436. DOI: 10.1175/2009JHM1182.1.

772 Giraudeau J (1993) Planktonic foraminiferal assemblages in surface sediments from the southwest
773 African continental margin. *Marine Geology* 110(1–2). Elsevier: 47–62. DOI: 10.1016/0025-
774 3227(93)90104-4.

775 Giraudeau J, Pierre C and Herve L (2001) *A Late Quaternary, High-resolution Record Of*
776 *Planktonic Foraminiferal Species Distribution in The Southern Benguela Region: SITE 1087*.
777 *Proceedings of the Ocean Drilling Program, Scientific Results*.

778 Giraudeau J, Grelaud M, Solignac S, et al. (2010) Millennial-scale variability in Atlantic water
779 advection to the Nordic Seas derived from Holocene coccolith concentration records.
780 *Quaternary Science Reviews* 29(9–10). Elsevier Ltd: 1276–1287. DOI:
781 10.1016/j.quascirev.2010.02.014.

782 Girone A, Maiorano P, Marino M, et al. (2013) Calcareous plankton response to orbital and
783 millennial-scale climate changes across the Middle Pleistocene in the western Mediterranean.

784 *Palaeogeography, Palaeoclimatology, Palaeoecology* 392. Elsevier: 105–116. DOI:
785 10.1016/J.PALAEO.2013.09.005.

786 Grelaud M, Beaufort L, Cuven S, et al. (2009) Glacial to interglacial primary production and El
787 Niño-Southern Oscillation dynamics inferred from coccolithophores of the Santa Barbara
788 Basin. *Paleoceanography* 24(1): 1–15. DOI: 10.1029/2007PA001578.

789 Hayes A, Kucera M, Kallel N, et al. (2005) Glacial Mediterranean sea surface temperatures based
790 on planktonic foraminiferal assemblages. *Quaternary Science Reviews* 24(7–9). Pergamon:
791 999–1016. DOI: 10.1016/J.QUASCIREV.2004.02.018.

792 Heburn GW and La Violette PE (1990) Variations in the structure of the anticyclonic gyres found in
793 the Alboran Sea. *Journal of Geophysical Research* 95(C2): 1599. DOI:
794 10.1029/JC095iC02p01599.

795 Hemleben C, Spindler M, Breitinger I, et al. (1985) *Field and laboratory studies on the ontogeny*
796 *and ecology of some globorotalid species from the Sargasso Sea off Bermuda*. *Journal of*
797 *Foraminiferal Research. v*.

798 Hemleben C, Spindler M and Anderson OR (1989) Taxonomy and Species Features. In: *Modern*
799 *Planktonic Foraminifera*. New York, NY: Springer New York, pp. 8–32. DOI: 10.1007/978-1-
800 4612-3544-6_2.

801 Hernández-Almeida I, Bárcena MA, Flores JA, et al. (2011) Microplankton response to
802 environmental conditions in the Alboran Sea (Western Mediterranean): One year sediment trap
803 record. *Marine Micropaleontology* 78(1–2). Elsevier: 14–24. DOI:
804 10.1016/J.MARMICRO.2010.09.005.

805 Hernández-Almeida I, Ausín B, Saavedra-Pellitero M, et al. (2019) Quantitative reconstruction of
806 primary productivity in low latitudes during the last glacial maximum and the mid-to-late
807 Holocene from a global Florisphaera profunda calibration dataset. *Quaternary Science Reviews*
808 205: 166–181. DOI: 10.1016/J.QUASCIREV.2018.12.016.

809 Howell MW and Thunell RC (1992) Organic carbon accumulation in Bannock Basin: Evaluating
810 the role of productivity in the formation of eastern Mediterranean sapropels. *Marine Geology*
811 103(1–3). Elsevier: 461–471. DOI: 10.1016/0025-3227(92)90032-D.

812 Huang NE, Shen Z, Long SR, et al. (1998) The empirical mode decomposition and Hilbert

spectrum for nonlinear and nonstationary time series analysis. *Proc. Roy. Soc. London* A454: 903–995.

Hurrell JW (1995) Decadal Trends in the North Atlantic Oscillation: Regional Temperatures and Precipitation. *Science* 269: 676–679.

Incarbona A, Sprovieri M, Di Stefano A, et al. (2013) Productivity modes in the mediterranean sea during dansgaard-oeschger (20,000-70,000yr ago) oscillations. *Palaeogeography, Palaeoclimatology, Palaeoecology* 392. Elsevier B.V.: 128–137. DOI: 10.1016/j.palaeo.2013.09.023.

Jalali B, Sicre M-A, Bassetti MA, et al. (2016) Holocene climate variability in the North-Western Mediterranean Sea (Gulf of Lions). *Climate of the Past* 12(1): 91–101. DOI: 10.5194/cp-12-91-2016.

Jalali B, Sicre M-A, Kallel N, et al. (2017) High-resolution Holocene climate and hydrological variability from two major Mediterranean deltas (Nile and Rhone). *Holocene* 27(8): 1158–1168. DOI: 10.1177/0959683616683258.

Jalut G, Esteban Amat A, Bonnet L, et al. (2000) Holocene climatic changes in the Western Mediterranean, from south-east France to south-east Spain. *Palaeogeography, Palaeoclimatology, Palaeoecology* 160(3–4): 255–290. DOI: 10.1016/S0031-0182(00)00075-4.

Jalut G, Dedoubat JJ, Fontugne M, et al. (2009) Holocene circum-Mediterranean vegetation changes: Climate forcing and human impact. *Quaternary International* 200(1–2): 4–18. DOI: 10.1016/j.quaint.2008.03.012.

Jiménez-Amat P and Zahn R (2015) Offset timing of climate oscillations during the last two glacial-interglacial transitions connected with large-scale freshwater perturbation. *Paleoceanography* 30(6): 768–788. DOI: 10.1002/2014PA002710.

Jimenez-Espejo FJ, Martinez-Ruiz F, Sakamoto T, et al. (2007) Paleoenvironmental changes in the western Mediterranean since the last glacial maximum: High resolution multiproxy record from the Algero-Balearic basin. *Palaeogeography, Palaeoclimatology, Palaeoecology* 246(2–4): 292–306. DOI: 10.1016/j.palaeo.2006.10.005.

Jimenez-Espejo FJ, Martinez-Ruiz F, Rogerson M, et al. (2008) Detrital input, productivity

842 fluctuations, and water mass circulation in the westernmost Mediterranean Sea since the Last
843 Glacial Maximum. *Geochemistry, Geophysics, Geosystems* 9(11). DOI:
844 10.1029/2008GC002096.

845 Jonkers L, Brummer G-JA, C Peeters FJ, et al. (2010) Seasonal stratification, shell flux, and oxygen
846 isotope dynamics of left-coiling. *Paleoceanography* 25. DOI: 10.1029/2009PA001849.

847 Jordan RW, Cros L and Young JR (2004) A revised classification scheme for living haptophytes.
848 *Micropaleontology* 50(Suppl_1). GeoScienceWorld: 55–79. DOI: 10.2113/50.Suppl_1.55.

849 Kallel N and Labeyrie L (1997) *Enhanced rainfall in the Mediterranean region during the last*
850 *Sapropel Event*. *Oceanologica Acta*.

851 Kallel N, Duplessy J-C, Labeyrie L, et al. (2000) Mediterranean pluvial periods and sapropel
852 formation over the last 200 000 years. *Palaeogeography, Palaeoclimatology, Palaeoecology*
853 157(1–2). Elsevier: 45–58. DOI: 10.1016/S0031-0182(99)00149-2.

854 Knappertsbusch M (1993) Geographic distribution of living and Holocene coccolithophores in the
855 Mediterranean Sea. *Marine Micropaleontology* 21(1–3). Elsevier: 219–247. DOI:
856 10.1016/0377-8398(93)90016-Q.

857 Kontakiotis G (2016) Late Quaternary paleoenvironmental reconstruction and paleoclimatic
858 implications of the Aegean Sea (eastern Mediterranean) based on paleoceanographic indexes
859 and stable isotopes. *Quaternary International* 401. Elsevier Ltd: 28–42. DOI:
860 10.1016/j.quaint.2015.07.039.

861 Kucera M, Weinelt Mara, Kiefer T, et al. (2005) Reconstruction of sea-surface temperatures from
862 assemblages of planktonic foraminifera: Multi-technique approach based on geographically
863 constrained calibration data sets and its application to glacial Atlantic and Pacific Oceans.
864 *Quaternary Science Reviews* 24(7-9 SPEC. ISS.). Pergamon: 951–998. DOI:
865 10.1016/j.quascirev.2004.07.014.

866 Kutzbach JE, He F, Vavrus SJ, et al. (2013) The dependence of equilibrium climate sensitivity on
867 climate state: Applications to studies of climates colder than present. *Geophysical Research*
868 *Letters* 40(14): 3721–3726. DOI: 10.1002/grl.50724.

869 Lambeck K, Rouby H, Purcell A, et al. (2014) Sea level and global ice volumes from the Last
870 Glacial Maximum to the Holocene. *Proceedings of the National Academy of Sciences* 111(43):

15296–15303. DOI: 10.1073/pnas.1411762111.

Laskar J, Robutel P, Joutel F, et al. (2004) A long-term numerical solution for the insolation quantities of the Earth. *Astronomy & Astrophysics* 428(1). EDP Sciences: 261–285. DOI: 10.1051/0004-6361:20041335.

Lionello P (2012) *The Climate of the Mediterranean Region From the Past to the Future*. DOI: 10.1016/B978-0-12-416042-2.00009-4.

Liquete C, Arnau P, Canals M, et al. (2005) Mediterranean river systems of Andalusia, southern Spain, and associated deltas: A source to sink approach. *Marine Geology* 222–223(1–4): 471–495. DOI: 10.1016/j.margeo.2005.06.033.

Lirer F, Sprovieri M, Ferraro L, et al. (2013) Integrated stratigraphy for the Late Quaternary in the eastern Tyrrhenian Sea. *Quaternary International* 292. Pergamon: 71–85. DOI: 10.1016/J.QUAINT.2012.08.2055.

Lobo FJ, Fernández-Salas LM, Moreno I, et al. (2006) The sea-floor morphology of a Mediterranean shelf fed by small rivers, northern Alboran Sea margin. *Continental Shelf Research* 26(20). Pergamon: 2607–2628. DOI: 10.1016/j.csr.2006.08.006.

Locarnini RA, Mishonov A V., Antonov JI, et al. (2013) World ocean atlas 2013. Volume 1, Temperature. DOI: 10.7289/V55X26VD.

Lomb NR (1976) Least-square frequency analysis of unequally spaced data. *Astrophys. Space Sci.* 29: 447–462.

Lowe JJ, Rasmussen SO, Björck S, et al. (2008) Synchronisation of palaeoenvironmental events in the North Atlantic region during the Last Termination: a revised protocol recommended by the INTIMATE group. *Quaternary Science Reviews* 27(1–2): 6–17. DOI: 10.1016/j.quascirev.2007.09.016.

Magny M, Miramont C and Sivan O (2002) Assessment of the impact of climate and anthropogenic factors on Holocene Mediterranean vegetation in Europe on the basis of palaeohydrological records. *Palaeogeography, Palaeoclimatology, Palaeoecology* 186(1–2). Elsevier: 47–59. DOI: 10.1016/S0031-0182(02)00442-X.

Magny M, Combourieu-Nebout N, De Beaulieu JL, et al. (2013) North-south palaeohydrological contrasts in the central mediterranean during the holocene: Tentative synthesis and working

900 hypotheses. *Climate of the Past* 9(5): 2043–2071. DOI: 10.5194/cp-9-2043-2013.

901 Margaritelli G, Vallefuoco M, Di Rita F, et al. (2016) Marine response to climate changes during
902 the last five millennia in the central Mediterranean Sea. *Global and Planetary Change* 142.
903 Elsevier: 53–72. DOI: 10.1016/J.GLOPLACHA.2016.04.007.

904 Marino M, Maiorano P, Tarantino F, et al. (2014) Coccolithophores as proxy of seawater changes at
905 orbital-to-millennial scale during middle Pleistocene Marine Isotope Stages 14-9 in North
906 Atlantic core MD01-2446. *Paleoceanography* 29(6). John Wiley & Sons, Ltd: 518–532. DOI:
907 10.1002/2013PA002574.

908 Martrat B, Grimalt JO, Lopez-Martinez C, et al. (2004) Abrupt temperature changes in the Western
909 Mediterranean over the past 250,000 years. *Science (New York, N.Y.)* 306(5702). American
910 Association for the Advancement of Science: 1762–5. DOI: 10.1126/science.1101706.

911 Martrat B, Jimenez-Amat P, Zahn R, et al. (2014) Similarities and dissimilarities between the last
912 two deglaciations and interglaciations in the North Atlantic region. *Quaternary Science*
913 *Reviews* 99(October 2016): 122–134. DOI: 10.1016/j.quascirev.2014.06.016.

914 Mayewski PA, Rohling EJ, Stager CJ, et al. (2004) Holocene climate variability. *Quaternary*
915 *Research* 62: 243–255. DOI: 10.1016/j.yqres.2004.07.001.

916 Meijer PT and Tuenter E (2007) The effect of precession-induced changes in the Mediterranean
917 freshwater budget on circulation at shallow and intermediate depth. *Journal of Marine Systems*
918 68(3–4). Elsevier: 349–365. DOI: 10.1016/J.JMARSYS.2007.01.006.

919 Mertens C and Schott F (1998) Interannual Variability of Deep-Water Formation in the
920 Northwestern Mediterranean. *journal of physical oceanography* 28: 1410–1428.

921 Millot C (2008) Short-term variability of the Mediterranean in- and out-flows. *Geophysical*
922 *Research Letters* 35(15). John Wiley & Sons, Ltd: L15603. DOI: 10.1029/2008GL033762.

923 Moreno A, Cacho I, Canals M, et al. (2004) Millennial-scale variability in the productivity signal
924 from the Alboran Sea record, Western Mediterranean Sea. *Palaeogeography,*
925 *Palaeoclimatology, Palaeoecology* 211(3–4). Elsevier: 205–219. DOI:
926 10.1016/J.PALAEO.2004.05.007.

927 Moreno A, Cacho I, Canals M, et al. (2005) Links between marine and atmospheric processes
928 oscillating on a millennial time-scale. A multi-proxy study of the last 50,000 yr from the

Alboran Sea (Western Mediterranean Sea). *Quaternary Science Reviews* 24(14–15): 1623–1636. DOI: 10.1016/j.quascirev.2004.06.018.

Moreno A, Pérez A, Frigola J, et al. (2012) The Medieval Climate Anomaly in the Iberian Peninsula reconstructed from marine and lake records. *Quaternary Science Reviews* 43. Elsevier Ltd: 16–32. DOI: 10.1016/j.quascirev.2012.04.007.

Moreno E, Thouveny N, Delanghe D, et al. (2002) Climatic and oceanographic changes in the Northeast Atlantic reflected by magnetic properties of sediments deposited on the Portuguese Margin during the last 340 ka. *Earth and Planetary Science Letters* 202(2). Elsevier: 465–480. DOI: 10.1016/S0012-821X(02)00787-2.

Munz PM, Siccha M, Lückge A, et al. (2015) Decadal-resolution record of winter monsoon intensity over the last two millennia from planktic foraminiferal assemblages in the northeastern Arabian Sea. *Holocene* 25(11). SAGE Publications Ltd: 1756–1771. DOI: 10.1177/0959683615591357.

Nieto-Moreno V, Martínez-Ruiz F, Giralt S, et al. (2011) Tracking climate variability in the western Mediterranean during the Late Holocene: A multiproxy approach. *Climate of the Past* 7(4): 1395–1414. DOI: 10.5194/cp-7-1395-2011.

Nieto-Moreno V, Martinez-Ruiz F, Gallego-Torres D, et al. (2015) Palaeoclimate and palaeoceanographic conditions in the westernmost Mediterranean over the last millennium: an integrated organic and inorganic approach. *Journal of the Geological Society* 172(2): 264–271. DOI: 10.1144/jgs2013-105.

Okada H and Wells P (1997) Late Quaternary nannofossil indicators of climate change in two deep-sea cores associated with the Leeuwin Current off Western Australia. *Palaeogeography, Palaeoclimatology, Palaeoecology* 131(3–4). Elsevier: 413–432. DOI: 10.1016/S0031-0182(97)00014-X.

Olsen J, Anderson NJ and Knudsen MF (2012) Variability of the North Atlantic Oscillation over the past 5,200 years. *Nature Geoscience* 5(11): 808–812. DOI: 10.1038/ngeo1589.

Oviedo AM, Ziveri P and Gazeau F (2017) Coccolithophore community response to increasing pCO2 in Mediterranean oligotrophic waters. *Estuarine, Coastal and Shelf Science* 186: 58–71. DOI: 10.1016/j.ecss.2015.12.007.

Pérez-Folgado M, Sierro FJ, Flores JA, et al. (2003) Western Mediterranean planktonic foraminifera events and millennial climatic variability during the last 70 kyr. *Marine Micropaleontology* 48(1–2). Elsevier: 49–70. DOI: 10.1016/S0377-8398(02)00160-3.

Pérez-Folgado M, Sierro FJ, Flores JA, et al. (2004) Paleoclimatic variations in foraminifer assemblages from the Alboran Sea (Western Mediterranean) during the last 150 ka in ODP Site 977. *Marine Geology* 212(1–4): 113–131. DOI: 10.1016/j.margeo.2004.08.002.

Perkins H, Kinder T and La Violette PE (1990) The Atlantic Inflow in the Western Alboran Sea. *Journal of Physical Oceanography* 20: 242–263.

Peyron O, Combourieu-Nebout N, Brayshaw D, et al. (2017) Precipitation changes in the Mediterranean basin during the Holocene from terrestrial and marine pollen records: A model-data comparison. *Climate of the Past* 13(3): 249–265. DOI: 10.5194/cp-13-249-2017.

Pflaumann U, Duprat J, Pujol C, et al. (1996) SIMMAX: A modern analog technique to deduce Atlantic sea surface temperatures from planktonic foraminifera in deep-sea sediments. *Paleoceanography* 11(1). John Wiley & Sons, Ltd: 15–35. DOI: 10.1029/95PA01743.

Piva A, Asioli A, Andersen N, et al. (2008) Climatic cycles as expressed in sediments of the PROMESS1 borehole PRAD1-2, central Adriatic, for the last 370 ka: 2. Paleoenvironmental evolution. *Geochemistry, Geophysics, Geosystems* 9(3). John Wiley & Sons, Ltd: n/a-n/a. DOI: 10.1029/2007GC001785.

Principato MS, Crudeli D, Ziveri P, et al. (2006) Phyto_ and zooplankton paleofluxes during the deposition of sapropel S1 (eastern Mediterranean): Biogenic carbonate preservation and paleoecological implications. *Palaeogeography, Palaeoclimatology, Palaeoecology* 235(1–3). Elsevier: 8–27. DOI: 10.1016/J.PALAEO.2005.09.021.

Pujol C and Vergnaud-Grazzini C (1995) Distribution patterns of live planktic foraminifers as related to regional hydrography and productive systems of the Mediterranean Sea. *Marine Micropaleontology* 25(2–3). Elsevier: 187–217. DOI: 10.1016/0377-8398(95)00002-I.

Ramos-Román MJ, Jiménez-Moreno G, Camuera J, et al. (2018) Millennial-scale cyclical environment and climate variability during the Holocene in the western Mediterranean region deduced from a new multi-proxy analysis from the Padul record (Sierra Nevada, Spain). *Global and Planetary Change* 168(June). Elsevier: 35–53. DOI: 10.1016/j.gloplacha.2018.06.003.

988 Rasmussen SO, Andersen KK, Svensson AM, et al. (2006) A new Greenland ice core chronology
989 for the last glacial termination. *Journal of Geophysical Research Atmospheres* 111(6): 1–16.
990 DOI: 10.1029/2005JD006079.

991 Repschläger J, Garbe-Schönberg D, Weinelt M, et al. (2017) Holocene evolution of the North
992 Atlantic subsurface transport. *Climate of the Past* 13(4): 333–344. DOI: 10.5194/cp-13-333-
993 2017.

994 Rigual-Hernández AS, Sierro FJ, Bárcena MA, et al. (2012) Seasonal and interannual changes of
995 planktic foraminiferal fluxes in the Gulf of Lions (NW Mediterranean) and their implications
996 for paleoceanographic studies: Two 12-year sediment trap records. *Deep Sea Research Part I:*
997 *Oceanographic Research Papers* 66. Pergamon: 26–40. DOI: 10.1016/J.DSR.2012.03.011.

998 Rixen M, Beckers JM, Levitus S, et al. (2005) The Western Mediterranean Deep Water: A proxy
999 for climate change. *Geophysical Research Letters* 32(12): 1–4. DOI: 10.1029/2005GL022702.

1000 Rodrigo-Gámiz M, Martínez-Ruiz F, Jiménez-Espejo FJ, et al. (2011) Impact of climate variability
1001 in the western Mediterranean during the last 20,000 years: Oceanic and atmospheric responses.
1002 *Quaternary Science Reviews* 30(15–16). Elsevier Ltd: 2018–2034. DOI:
1003 10.1016/j.quascirev.2011.05.011.

1004 Rogerson M, Cacho I, Jimenez-Espejo FJ, et al. (2008) A dynamic explanation for the origin of the
1005 western Mediterranean organic-rich layers. *Geochemistry, Geophysics, Geosystems* 9(7). John
1006 Wiley & Sons, Ltd: n/a-n/a. DOI: 10.1029/2007GC001936.

1007 Rohling EJ and Pälike H (2005) Centennial-scale climate cooling with a sudden cold event around
1008 8,200 years ago. *Nature* 434(7036): 975–979. DOI: 10.1038/nature03421.

1009 Rohling EJ, Den Dulk M, Pujol C, et al. (1995) Abrupt hydrographic change in the Alboran Sea
1010 (western Mediterranean) around 8000 yrs BP. *Deep-Sea Research Part I* 42(9): 1609–1619.
1011 DOI: 10.1016/0967-0637(95)00069-I.

1012 Rohling EJ, Jorissen FJ and De Stigter HC (1997) 200 Year interruption of Holocene sapropel
1013 formation in the Adriatic Sea. *Journal of Micropalaeontology* 16(2): 97–108. DOI:
1014 10.1144/jm.16.2.97.

1015 Rohling EJ, Cane TR, Cooke S, et al. (2002) African monsoon variability during the previous
1016 interglacial maximum. *Earth and Planetary Science Letters* 202(1). Elsevier: 61–75. DOI:

1017 10.1016/S0012-821X(02)00775-6.

1018 Rohling EJ, Sprovieri M, Cane T, et al. (2004) Reconstructing past planktic foraminiferal habitats
1019 using stable isotope data: a case history for Mediterranean sapropel S5. *Marine*
1020 *Micropaleontology* 50(1–2). Elsevier: 89–123. DOI: 10.1016/S0377-8398(03)00068-9.

1021 Rohling EJ, Marino G and Grant KM (2015) Mediterranean climate and oceanography, and the
1022 periodic development of anoxic events (sapropels). *Earth-Science Reviews* 143. Elsevier B.V.:
1023 62–97. DOI: 10.1016/j.earscirev.2015.01.008.

1024 Rossignol-Strick M (1985) Mediterranean Quaternary sapropels, an immediate response of the
1025 African monsoon to variation of insolation. *Palaeogeography, Palaeoclimatology,*
1026 *Palaeoecology* 49(3–4). Elsevier: 237–263. DOI: 10.1016/0031-0182(85)90056-2.

1027 Rossignol-Strick M, Nesteroff W, Olive P, et al. (1982) After the deluge: Mediterranean stagnation
1028 and sapropel formation. *Nature* 295(5845). Nature Publishing Group: 105–110. DOI:
1029 10.1038/295105a0.

1030 Salgueiro E, Voelker AHL, de Abreu L, et al. (2010) Temperature and productivity changes off the
1031 western Iberian margin during the last 150 ky. *Quaternary Science Reviews* 29(5–6).
1032 Pergamon: 680–695. DOI: 10.1016/J.QUASCIREV.2009.11.013.

1033 Salgueiro E, Naughton F, Voelker AHL, et al. (2014) Past circulation along the western Iberian
1034 margin: A time slice vision from the Last Glacial to the Holocene. *Quaternary Science*
1035 *Reviews* 106: 316–329. DOI: 10.1016/j.quascirev.2014.09.001.

1036 Sarhan T, García-Lafuente J, Vargas M, et al. (2000) Upwelling mechanisms in the northwestern
1037 Alboran Sea. *Journal of Marine Systems* 23(4): 317–331. DOI: 10.1016/S0924-
1038 7963(99)00068-8.

1039 Sbaffi L, Wezel FC, Kallel N, et al. (2001) Response of the pelagic environment to palaeoclimatic
1040 changes in the central Mediterranean Sea during the Late Quaternary. *Marine Geology* 178(1–
1041 4): 39–62. DOI: 10.1016/S0025-3227(01)00185-2.

1042 Scargle JD (1982) Studies in astronomical time series analysis, II Statistical aspects of spectral
1043 analysis of unevenly spaced data. *Astrophys. J.* 263: 835–853.

1044 Schiebel R, Waniek J, Bork M, et al. (2001) Planktic foraminiferal production stimulated by
1045 chlorophyll redistribution and entrainment of nutrients. *Deep Sea Research Part I:*

Oceanographic Research Papers 48(3). Pergamon: 721–740. DOI: 10.1016/S0967-0637(00)00065-0.

Schirrmacher J, Weinelt M, Blanz T, et al. (2019) Multi-decadal climate variability in southern Iberia during the mid- to late-Holocene. *Climate of the Past Discussions*: 1–29. DOI: 10.5194/cp-2018-158.

Schulz M and Mudelsee M (2002) REDFIT: estimating red-noise spectra directly from unevenly spaced paleoclimatic time series. *Comput. Geosci.* 28: 421–426.

Siccha M, Trommer G, Schulz H, et al. (2009) Factors controlling the distribution of planktonic foraminifera in the Red Sea and implications for the development of transfer functions. *Marine Micropaleontology* 72(3–4). Elsevier: 146–156. DOI: 10.1016/J.MARMICRO.2009.04.002.

Sierro FJ, Hodell DA, Curtis JH, et al. (2005) Impact of iceberg melting on Mediterranean thermohaline circulation during Heinrich events. *Paleoceanography* 20(2): 1–13. DOI: 10.1029/2004PA001051.

Smith AC, Wynn PM, Barker PA, et al. (2016) North Atlantic forcing of moisture delivery to Europe throughout the Holocene. *Scientific Reports* 6. Nature Publishing Group: 1–7. DOI: 10.1038/srep24745.

Smith RO, Bryden HL and Stansfield K (2008) *Observations of new western Mediterranean deep water formation using Argo floats*. *Ocean Sci*.

Spezzaferri S, Kucera M, Pearson PN, et al. (2015) Fossil and Genetic Evidence for the Polyphyletic Nature of the Planktonic Foraminifera 'Globigerinoides', and Description of the New Genus Trilobatus. Abramovich S (ed.) *PLOS ONE* 10(5). Public Library of Science. DOI: 10.1371/journal.pone.0128108.

Sprovieri M, Di Stefano E, Incarbona A, et al. (2012) Centennial- to millennial-scale climate oscillations in the Central-Eastern Mediterranean Sea between 20,000 and 70,000 years ago: Evidence from a high-resolution geochemical and micropaleontological record. *Quaternary Science Reviews* 46: 126–135. DOI: 10.1016/j.quascirev.2012.05.005.

Sprovieri R, Di Stefano E, Incarbona A, et al. (2003) A high-resolution record of the last deglaciation in the Sicily Channel based on foraminifera and calcareous nannofossil quantitative distribution. *Palaeogeography, Palaeoclimatology, Palaeoecology* 202(1–2): 119–

142. DOI: 10.1016/S0031-0182(03)00632-1.

Steinmetz JC (1994) Sedimentation of Coccolithophores. In: *Coccolithophores*, pp. 179–183.

Stolz K and Baumann K-H (2010) Changes in palaeoceanography and palaeoecology during Marine Isotope Stage (MIS) 5 in the eastern North Atlantic (ODP Site 980) deduced from calcareous nannoplankton observations. *Palaeogeography, Palaeoclimatology, Palaeoecology* 292(1–2). Elsevier B.V.: 295–305. DOI: 10.1016/j.palaeo.2010.04.002.

Sumner G, Homar V and Ramis C (2001) Precipitation seasonality in eastern and southern coastal Spain. *International Journal of Climatology* 21(2). John Wiley & Sons, Ltd: 219–247. DOI: 10.1002/joc.600.

Takahashi K and Okada H (2000) Environmental control on the biogeography of modern coccolithophores in the southeastern Indian Ocean offshore of Western Australia. *Marine Micropaleontology* 39(1–4): 73–86. DOI: 10.1016/S0377-8398(00)00015-3.

Thornalley DJR, Elderfield H and McCave N (2009) Holocene oscillations in temperature and salinity of the surface subpolar North Atlantic. *Nature* 457. Nature Publishing Group: 711–713. DOI: 10.1038/nature07717.

Toucanne S, Zaragosi S, Bourillet J-F, et al. (2012) External controls on turbidite sedimentation on the glacially-influenced Armorican margin (Bay of Biscay, western European margin). *Marine Geology* 303–306. Elsevier: 137–153. DOI: 10.1016/J.MARGEO.2012.02.008.

Toucanne S, Angue Minto'o CM, Fontanier C, et al. (2015) Tracking rainfall in the northern Mediterranean borderlands during sapropel deposition. *Quaternary Science Reviews* 129. Pergamon: 178–195. DOI: 10.1016/J.QUASCIREV.2015.10.016.

Triantaphyllou M, Antonarakou A, Dimiza M, et al. (2010) Calcareous nannofossil and planktonic foraminiferal distributional patterns during deposition of sapropels S6, S5 and S1 in the Libyan Sea (Eastern Mediterranean). *Geo-Marine Letters* 30(1): 1–13. DOI: 10.1007/s00367-009-0145-7.

Trigo R, Pozo-Vázquez D, Osborn TJ, et al. (2004) North Atlantic oscillation influence on precipitation, river flow and water resources in the Iberian Peninsula. *International Journal of Climatology* 24(8): 925–944. DOI: 10.1002/joc.1048.

Tzedakis PC (2007) Seven ambiguities in the Mediterranean palaeoenvironmental narrative.

Quaternary Science Reviews 26(17–18). Pergamon: 2042–2066. DOI: 10.1016/J.QUASCIREV.2007.03.014.

Vallefuoco M, Lirer F, Ferraro L, et al. (2012) Climatic variability and anthropogenic signatures in the Gulf of Salerno (southern-eastern Tyrrhenian Sea) during the last half millennium. *Rendiconti Lincei* 23(1). Springer Milan: 13–23. DOI: 10.1007/s12210-011-0154-0.

Vargas-Yáñez M, Jesús García M, Salat J, et al. (2008) Warming trends and decadal variability in the Western Mediterranean shelf. *Global and Planetary Change* 63(2–3). Elsevier: 177–184. DOI: 10.1016/J.GLOPLACHA.2007.09.001.

Vincent E and Berger WH (1981) Planktonic foraminifera and their use in paleoceanography. *The Sea* 7: 371–412.

Viúdez Á, Tintoré J, Haney RL, et al. (1996) Circulation in the Alboran Sea as Determined by Quasi-Synoptic Hydrographic Observations. Part I: Three-Dimensional Structure of the Two Anticyclonic Gyres. *Journal of Physical Oceanography* 26(5): 684–705. DOI: 10.1175/1520-0485(1996)026<0684:CITASA>2.0.CO;2.

Walker MJC, Berkelhammer M, Björck S, et al. (2012) Formal subdivision of the Holocene Series/Epoch: A Discussion Paper by a Working Group of INTIMATE (Integration of ice-core, marine and terrestrial records) and the Subcommission on Quaternary Stratigraphy (International Commission on Stratigraphy). *Journal of Quaternary Science* 27(7): 649–659. DOI: 10.1002/jqs.2565.

Wanner H, Mercolli L, Grosjean M, et al. (2015) Holocene climate variability and change; a data-based review. *Journal of the Geological Society* 172(2): 254–263. DOI: 10.1144/jgs2013-101.

Weaver PPE and Pujol C (1988) History of the last deglaciation in the alboran sea (western Mediterranean) and adjacent north Atlantic as revealed by coccolith floras. *Palaeogeography, Palaeoclimatology, Palaeoecology* 64(1–2): 35–42. DOI: 10.1016/0031-0182(88)90140-X.

Winter A and Siesser WG (1994) *Coccolithophores*. Cambridge University Press.

Young J, Geisen M, Cros L, et al. (2003) A guide to extant coccolithophore taxonomy. *Journal of Nannoplankton Research Special Issue* 1.

Zachariasse W-J, Jorissen FJ, Perissoratis C, et al. (1997) Late Quaternary foraminiferal changes and the nature of Sapropel S1 in Skopelos Basin. *Proceeding of the 5th Hellenic Symposium*

on Oceanography and Fisheries 1: 391–394.

Zanchetta G, Drysdale RN, Hellstrom JC, et al. (2007) Enhanced rainfall in the Western Mediterranean during deposition of sapropel S1: stalagmite evidence from Corchia cave (Central Italy). *Quaternary Science Reviews* 26(3–4): 279–286. DOI: 10.1016/j.quascirev.2006.12.003.

Zielhofer C, Fletcher WJ, Mischke S, et al. (2017) Atlantic forcing of Western Mediterranean winter rain minima during the last 12,000 years. *Quaternary Science Reviews* 157. Elsevier Ltd: 29–51. DOI: 10.1016/j.quascirev.2016.11.037.

Figure captions

Fig. 1: Location of ODP Site 976 in the Alboran Sea (western Mediterranean), bathymetry of the area and modern-day oceanographic circulation. **AW** (Atlantic Water); **MOW** (Mediterranean Outflow Water); **WMDW** (western Mediterranean Deep Water); **LIW** (Levantine Intermediate Water); **WAG** (western Alboran Gyre); **EAG** (eastern Alboran Gyre). In violet shade: Alboran and Almeria-Oran upwelling fronts

Fig. 2: Downcore variations of calcareous nannofossil assemblages at Site 976 plotted as relative abundance (%, black line) and nannofossil accumulation rate - NAR (coccolith/cm^2 kyr, filled area). Sedimentation rate over time used for NAR calculation, from Martrat et al. (2014), is also shown. YD: Younger Dryas.

Fig. 3: Downcore variations of planktonic foraminifera assemblages at Site 976 plotted as relative abundance (%, black line) and planktonic foraminifera accumulation rate – pfAR (forams/cm^{2}kyr, filled area), together with foraminifera-based summer, winter and annual SST and similarity index. Sedimentation rate over time, used for pfAR calculation, from Martrat et al. (2014). YD: Younger Dryas.

Fig. 4:(a) Signal of the Total NAR decomposed with CEEMD in five IMFs plus a residue (trend); (b), (c), (d), (e) spectral analysis made with "REDFIT" and Foster's WWZ, of the IMFs extracted from Total NAR. The green and black line represent the 95% and 80% Confident Level respectively. Significantly periodicity (red dot) and relative values expressed in years were

reported.

Fig. 5: Abundances variations of calcareous plankton assemblage and additional proxies from Site 976: accumulation rate of selected coccolithophores and planktonic foraminifera; relative abundance patterns of selected pollen taxa at Site 976 from Combourieu-Nebout et al. (2009); black line, 3 point average. Di- and tri-unsaturated alkenones of 37 carbons (C_{37}) from Martrat et al. (2014) and summer insolation curve (Laskar et al., 2004) are also shown. Younger Dryas (YD, grey bar); 8.2 ka event (light blue bar); dashed black lines are used to trace boundaries among phases I-III.

Fig. 6: Abundances variations of calcareous plankton assemblage and additional proxies from Site 976: accumulation rate of selected coccolithophores and planktonic foraminifera; black line, 3 point average; foram based seasonal SST variations at Site 976; relative abundance patterns of selected pollen taxa at Site 976 from Combourieu-Nebout et al. (2009). 8.2 ka event (dotted bar), dashed black lines are used to trace boundaries among phases I-III.

Fig. 7: Abundances variation of coccolithophore assemblage and climate proxies from Site 976: *G. oceanica* absolute abundances (black line, 3 point average); $\delta^{18}O_{seawater}$ at Site 976 (green line, 3 point average) (Jimenez-Amat and Zahn, 2015); $\delta^{18}O$ of combined and de-trended speleothems from Iberian Peninsula (Smith et al., 2016); coccolithophore productivity (total Nannofossil Accumulation Rate) at Site 976 (black line, 3 point average). Inferred NAO circulation pattern from redox variability from Lake SS1220, Greenland (Olsen et al., 2012) is also shown. Light blue bars represent periods of increased total NAR concomitant with enhanced Atlantic inflow and positive NAO index phases.

Fig. 8: Proposed different NAO circulations pattern scenarios as explained in the text: a) **NAO+** enhanced northwesterly winds, deep water formation and Atlantic inflow inducing upwelling and coccolithophore productivity; b) **NAO-** reduced northwesterly winds, deep water formation and Atlantic inflow, inducing stratification and reduced coccolithophore productivity. **LIW** (Levantine Intermediate Water). **AJ** (Atlantic Jet); **WMDW** (western Mediterranean Deep Water). **MOW** (Mediterranean Outflow Water). Diagram not to scale.

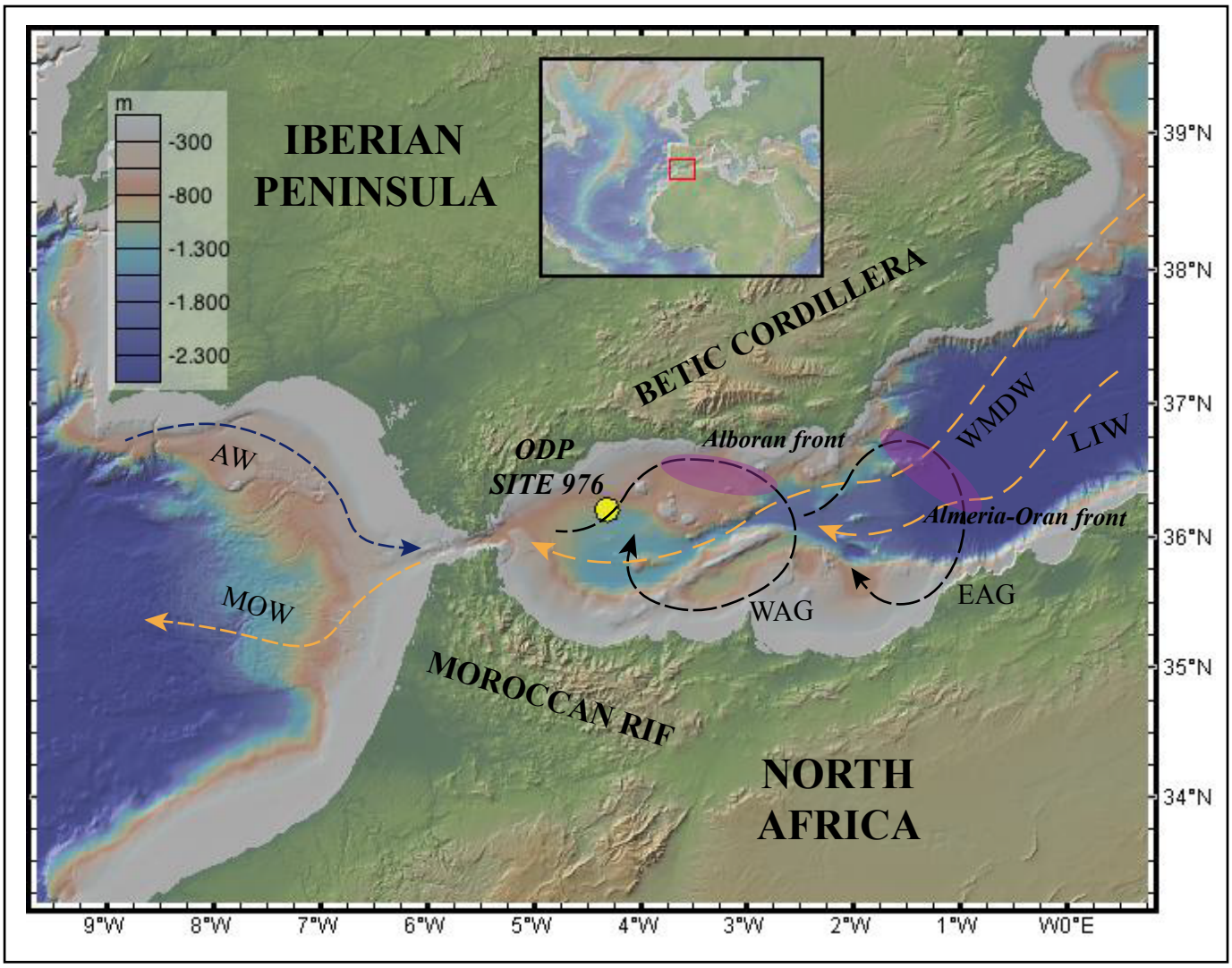
m
-300
-800
-1.300
-1.800
-2.300
IBERIAN PENINSULA
BETIC CORDILLERA
AW
MOW
ODP SITE 976
Alboran front
WMDW
LIW
Almeria-Oran front
WAG
EAG
MOROCCAN RIF
NORTH AFRICA
39°N
38°N
37°N
36°N
35°N
34°N
9°W
8°W
7°W
6°W
5°W
4°W
3°W
2°W
1°W
W0°E

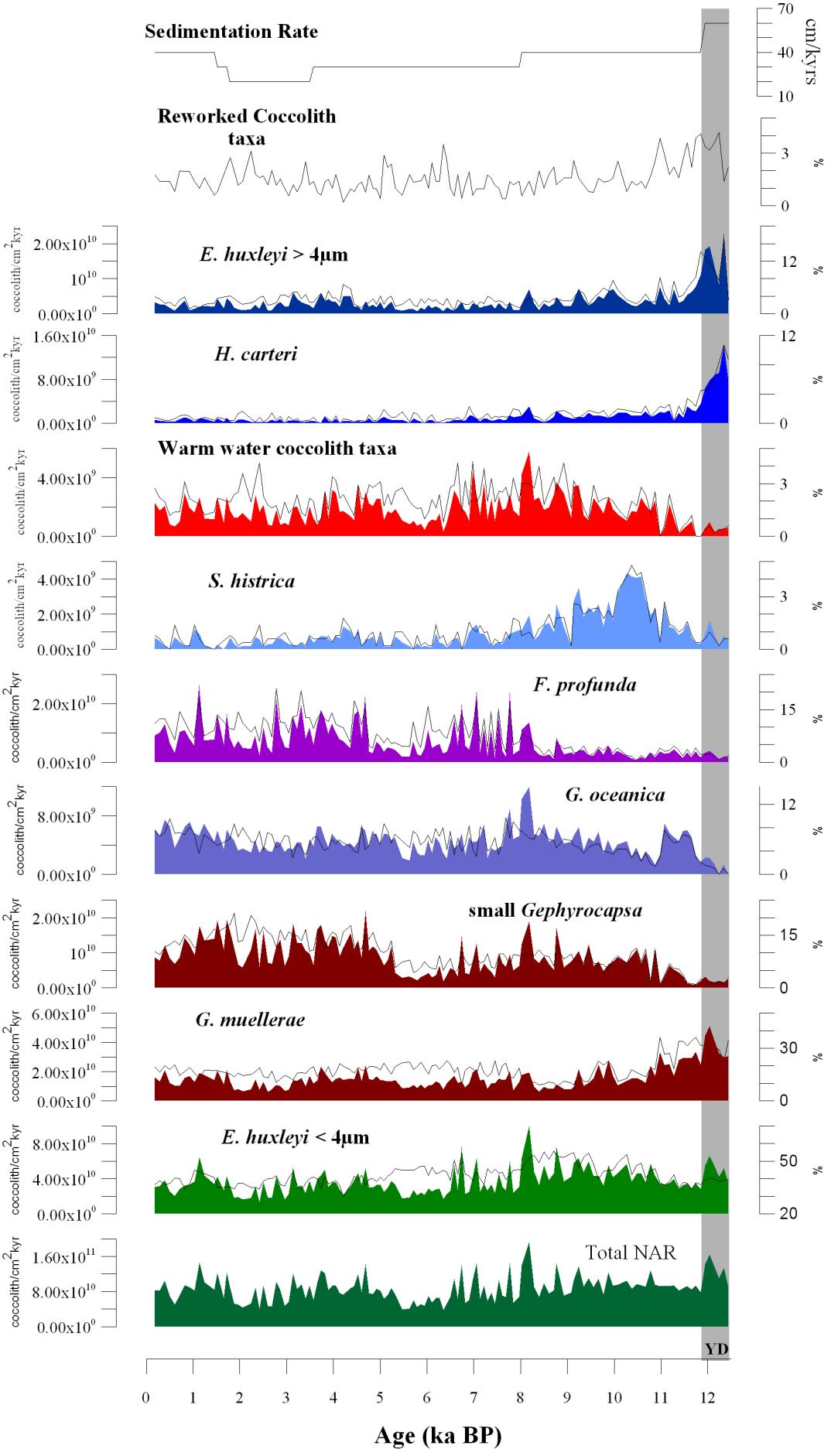
Sedimentation Rate
70
40
10
cm/kyrs
Reworked Coccolith taxa
3
0
%
E. huxleyi > 4µm
coccolith/cm²kyr
2.00x10¹⁰
10¹⁰
0.00x10⁰
12
0
H. carteri
1.60x10¹⁰
8.00x10⁹
Warm water coccolith taxa
4.00x10⁹
S. histrica
2.00x10⁹
F. profunda
15
G. oceanica
small Gephyrocapsa
G. muellerae
6.00x10¹⁰
4.00x10¹⁰
30
E. huxleyi < 4µm
8.00x10¹⁰
50
20
Total NAR
1.60x10¹¹
8.00x10¹⁰
YD
0 1 2 3 4 5 6 7 8 9 10 11 12
Age (ka BP)

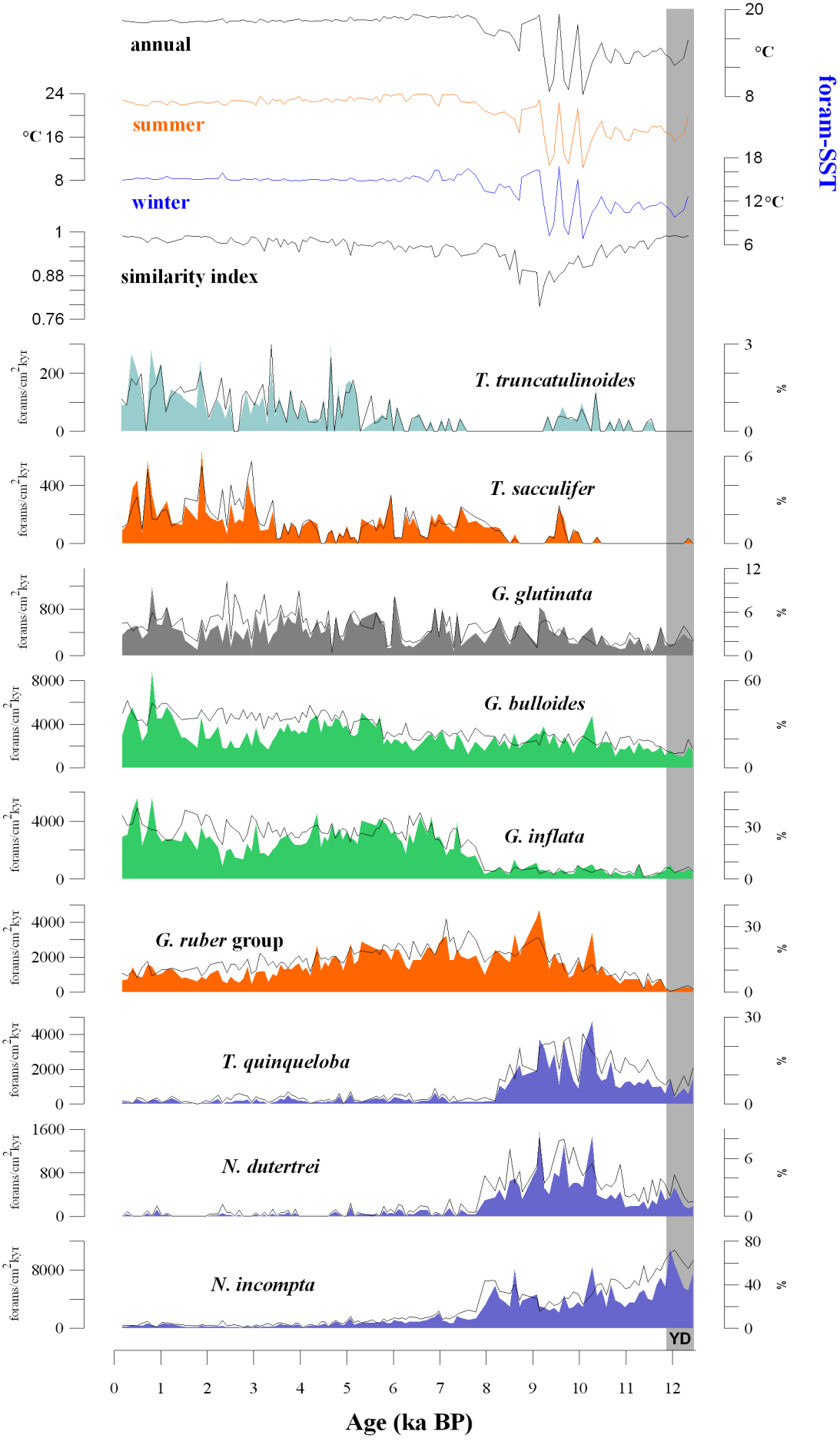
annual
summer
winter
similarity index
°C
foram-SST
T. truncatulinoides
T. sacculifer
G. glutinata
G. bulloides
G. inflata
G. ruber group
T. quinqueloba
N. dutertrei
N. incompta
foraminifera/cm²kyr
%
YD
Age (ka BP)

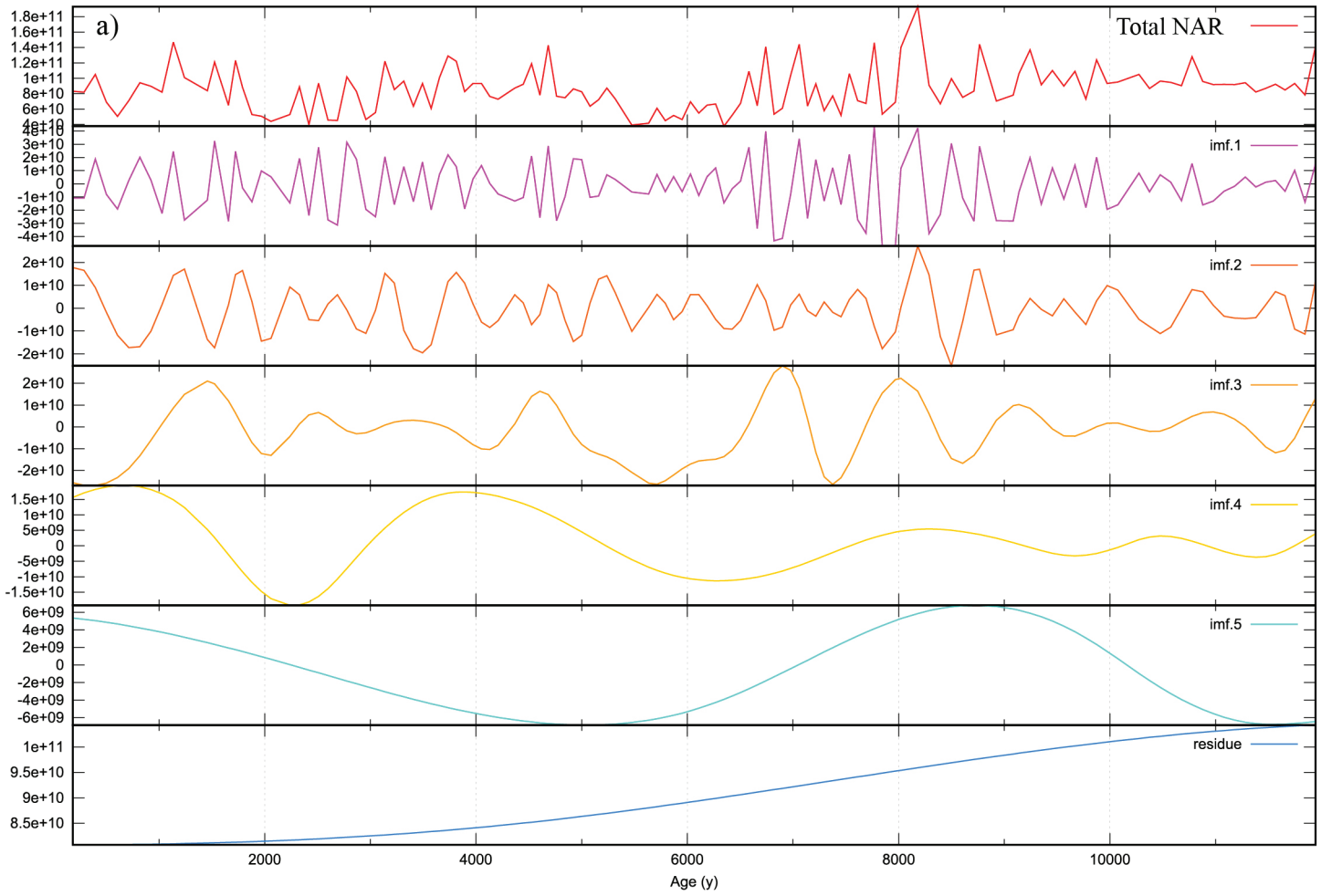

Total NAR IMF2

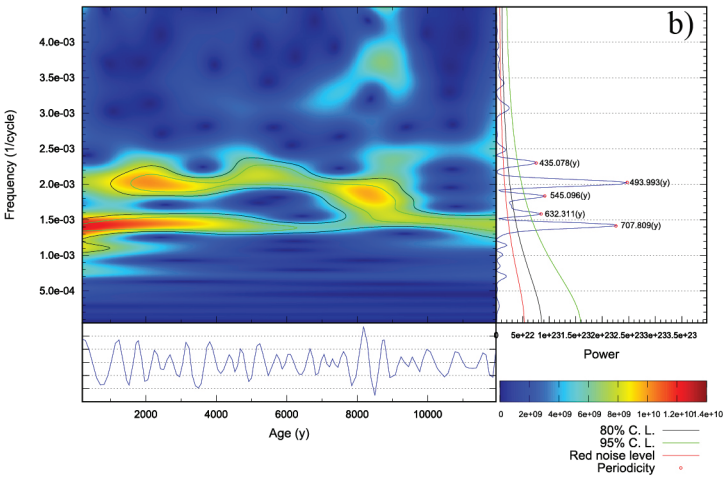

Total NAR IMF3

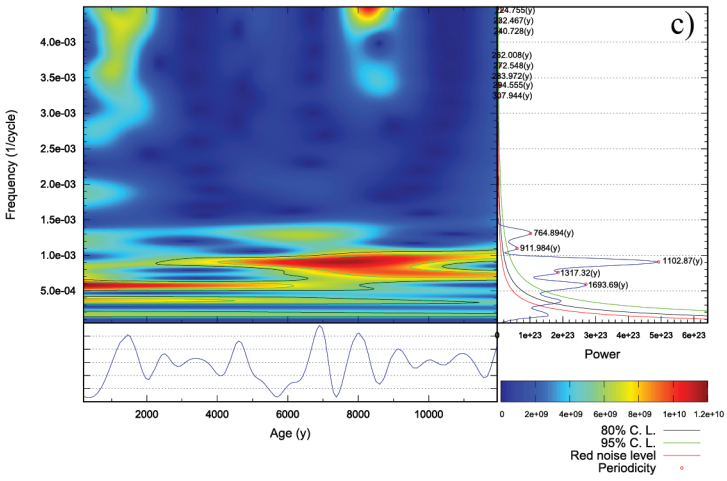

Total NAR IMF4

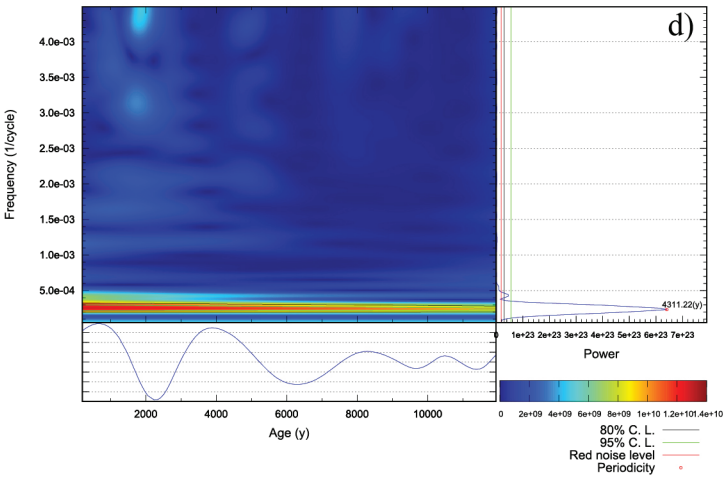

Total NAR IMF5

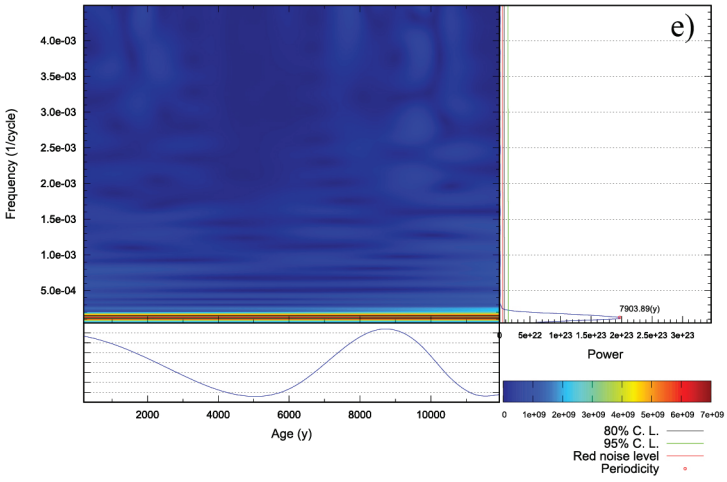

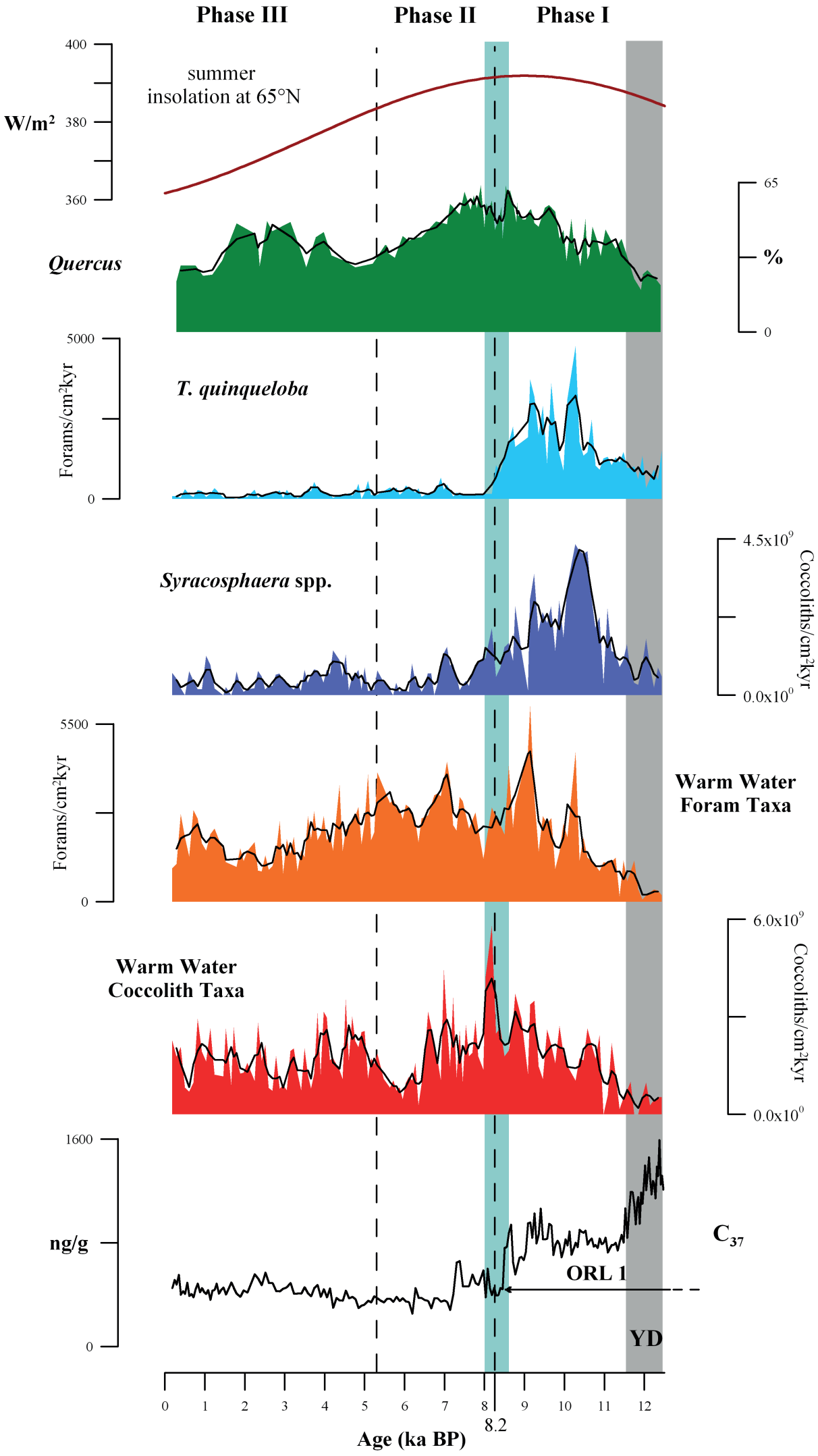
Phase III
Phase II
Phase I
summer
insolation at 65°N
W/m²
400
380
360
Quercus
65
%
0
5000
Forams/cm²kyr
0
T. quinqueloba
Syracosphaera spp.
4.5x10⁹
0.0x10⁰
Coccoliths/cm²kyr
5500
Forams/cm²kyr
0
Warm Water
Foram Taxa
Warm Water
Coccolith Taxa
6.0x10⁹
0.0x10⁰
Coccoliths/cm²kyr
1600
ng/g
0
C37
ORL 1
YD
0
1
2
3
4
5
6
7
8
9
10
11
12
8.2
Age (ka BP)

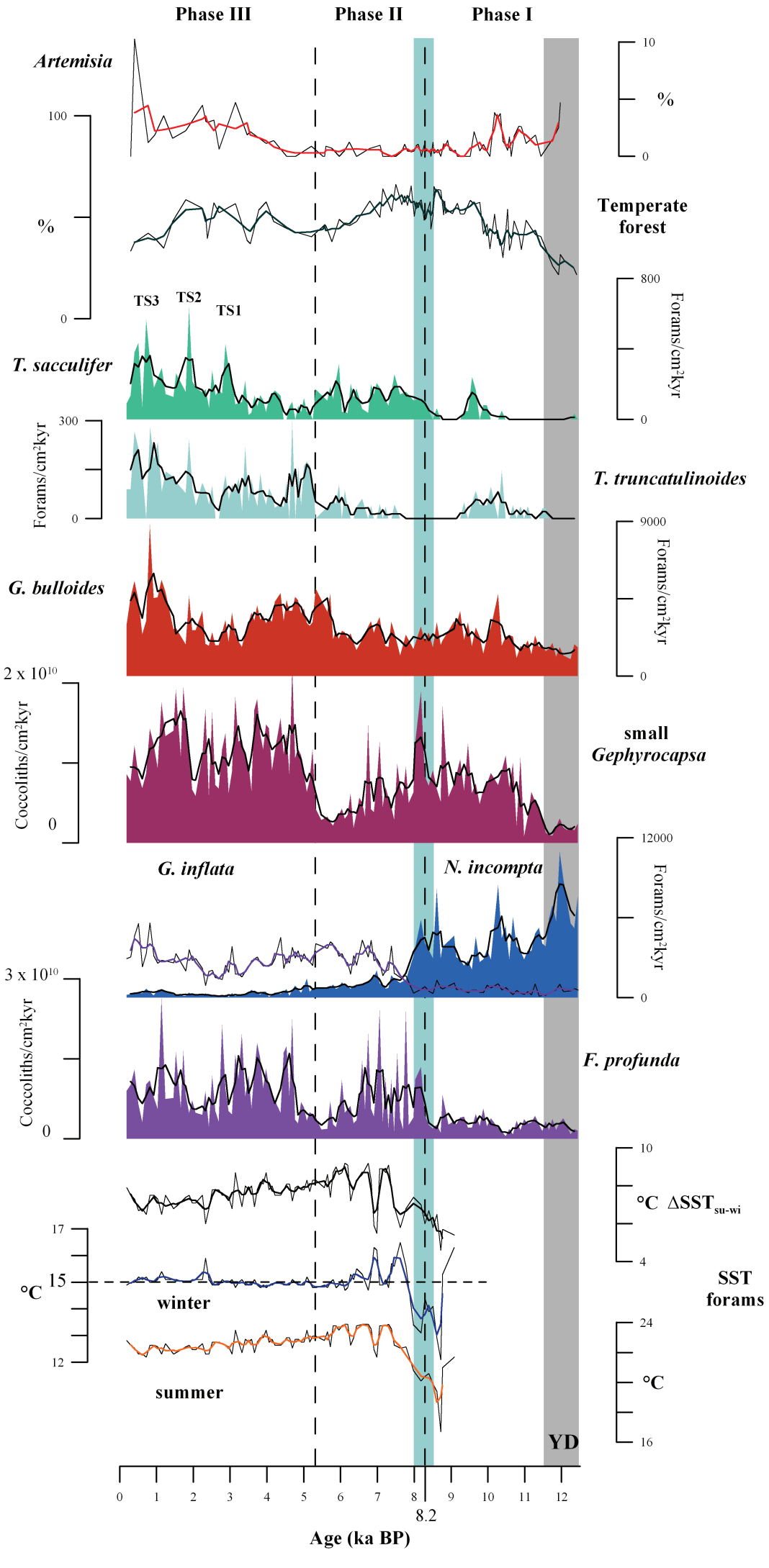
Phase III
Phase II
Phase I
Artemisia
100
%
0
10
%
0
Temperate forest
TS3
TS2
TS1
T. sacculifer
800
Forams/cm²kyr
0
300
Forams/cm²kyr
0
T. truncatulinoides
G. bulloides
9000
Forams/cm²kyr
0
2 x 10¹⁰
Coccoliths/cm²kyr
0
small Gephyrocapsa
G. inflata
N. incompta
12000
Forams/cm²kyr
0
3 x 10¹⁰
Coccoliths/cm²kyr
0
F. profunda
10
°C ΔSST su-wi
4
SST foram
17
°C
15
12
winter
summer
24
°C
16
YD
0
1
2
3
4
5
6
7
8
9
10
11
12
8.2
Age (ka BP)

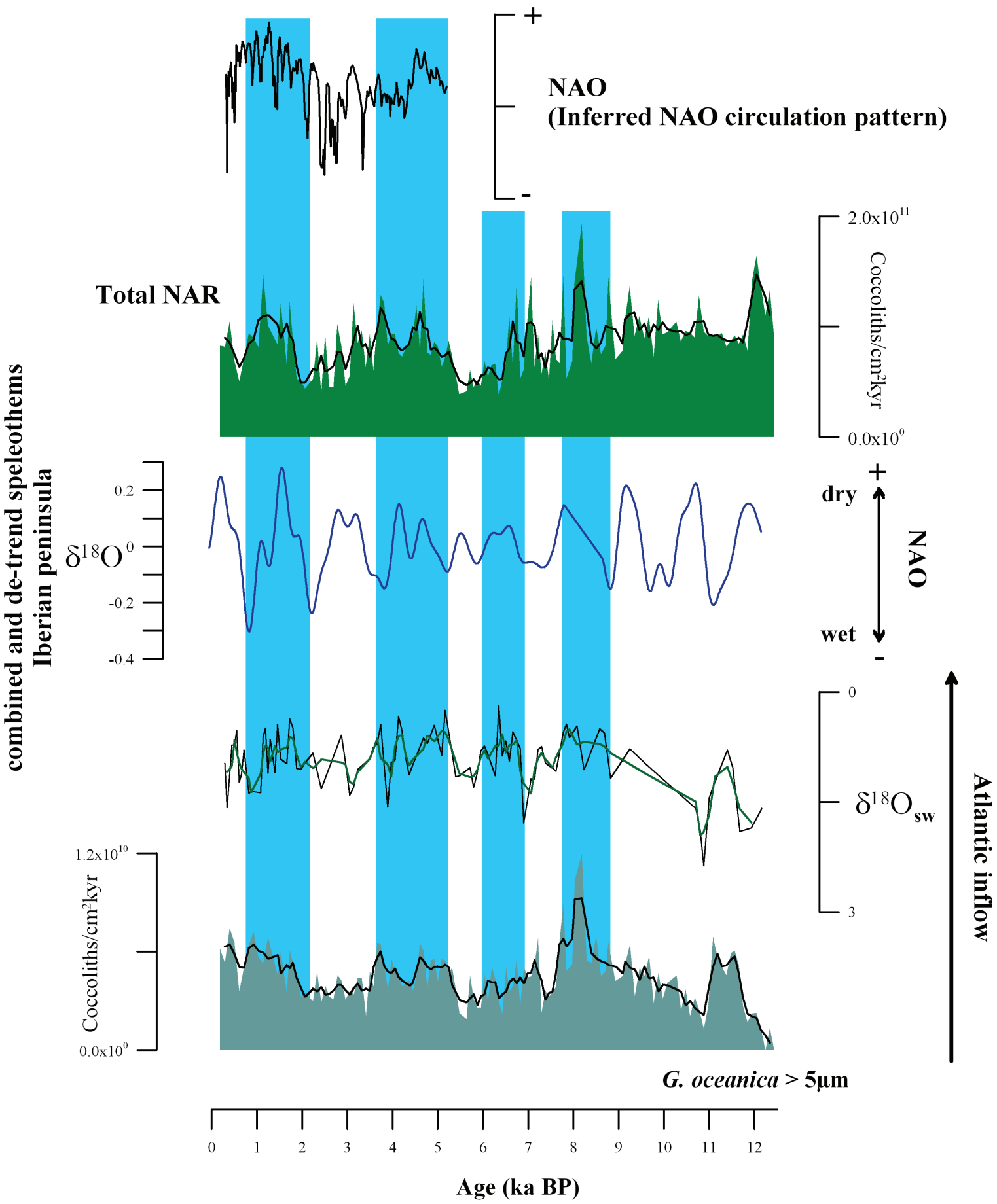
+
NAO
(Inferred NAO circulation pattern)
-
Total NAR
2.0x10^11
Coccoliths/cm²kyr
0.0x10^0
combined and de-trend speleothems
Iberian peninsula
0.2
δ18O 0
-0.2
-0.4
+
dry
NAO
wet
-
0
δ18Osw
3
Atlantic inflow
1.2x10^10
Coccoliths/cm²kyr
0.0x10^0
G. oceanica > 5µm
0 1 2 3 4 5 6 7 8 9 10 11 12
Age (ka BP)

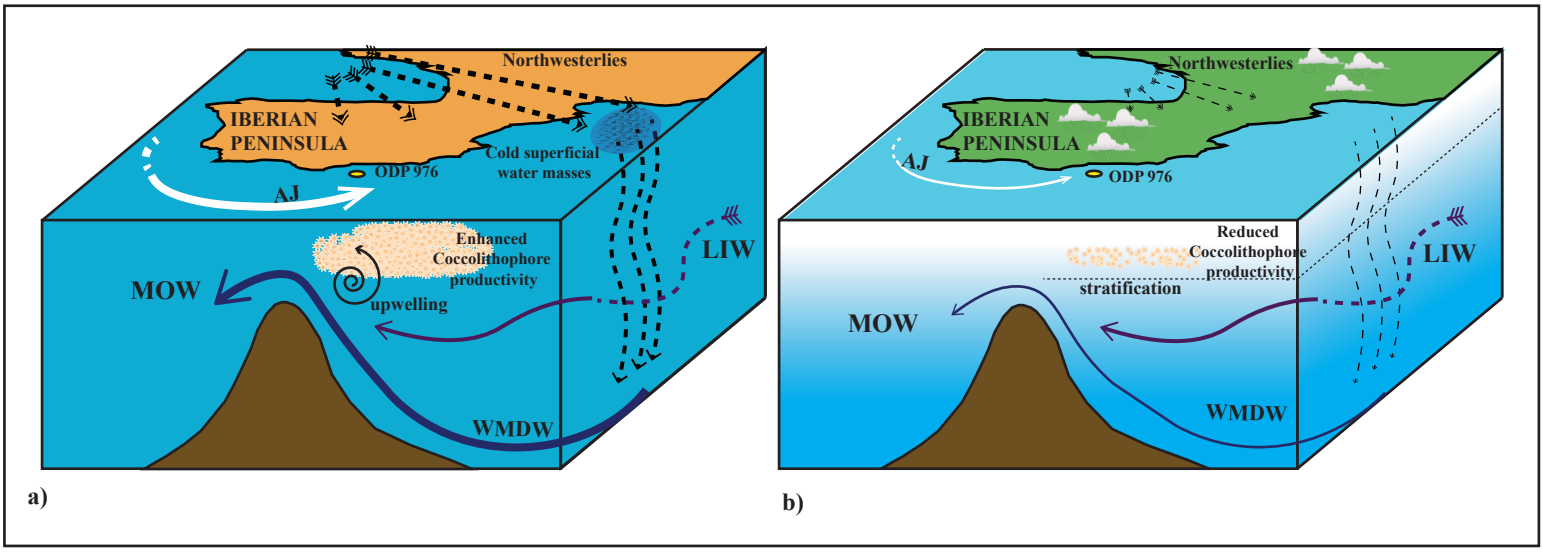
Northwesterlies
IBERIAN PENINSULA
ODP 976
Cold superficial water masses
AJ
Enhanced Coccolithophore productivity
upwelling
MOW
LIW
WMDW
a)
Northwesterlies
IBERIAN PENINSULA
AJ
ODP 976
Reduced Coccolithophore productivity
stratification
MOW
LIW
WMDW
b)